UNIVERSITAT POLITÈCNICA DE VALÈNCIA

ESCOLA POLITECNICA SUPERIOR DE GANDIA

MÁSTER UNIVERSITARIO EN EVALUACIÓN Y SEGUIMIENTO AMBIENTAL DE ECOSISTEMAS MARINOS Y COSTEROS

UNIVERSITAT
POLITÈCNICA
DE VALÈNCIA

ESCOLA POLITÈCNICA
SUPERIOR DE GANDIA

"Analysis of the evolution of sea water quality in the Spanish coast from satellite images before and during the quarantine caused by COVID-19"

TRABAJO FINAL DE MÁSTER

Autor/a:
Mar Parra Boronat

Tutor/a:
Jaime Lloret Maurí
Lorena Parra Boronat

GANDIA, 2020

Abstract:

Satellite imaging is a form of remote sensing which can be used for several ecological purposes. Remote sensing has been used even to analyze water quality. There are many indexes which use the values from different bands to calculate environmental parameters. This project studies the effect the COVID-19 quarantine in Spain had on the Alboran Sea. The changes in water quality before (since February 3rd) and during (until June 22nd) the quarantine are analyzed in this essay. The dynamics studied are relevant for environmental restoration purposes. Already existing indices are applied using both ArcGIS and ACOLITE to determine several environmental parameters. Colored dissolved organic matter, suspended particulate matter, chlorophyll a and harmful algal blooms are the parameters studied in this project. The results show the effect storms had since they create massive overland flows, as well as the evolution of the concentrations after such events. To do so, the results are compared with weather tables. Furthermore, the existence of a correlation between the parameters (except for the harmful algal blooms) is presented. Moreover, it proves the effect a sudden human impact has on an ecosystem which has been unperturbed for a few months.

Keywords: colored dissolved organic matter, suspended particulate matter, chlorophyll a, harmful algal blooms, remote sensing

Resumen:

Las imágenes satelitales son una forma de teledetección que se puede utilizar para varios fines ecológicos. La teledetección ha sido utilizada incluso para analizar la calidad del agua. Hay muchos índices que utilizan los valores de diferentes bandas para calcular parámetros ambientales. Este TFM estudia el efecto de la cuarentena del COVID-19 en España en el Mar de Alborán. En este ensayo se analizan los cambios en la calidad del agua antes (desde el 3 de febrero) y durante (hasta el 22 de junio) la cuarentena. Las dinámicas estudiadas son relevantes para fines de restauración ambiental. Los índices ya existentes se aplican utilizando ArcGIS y ACOLITE para determinar varios parámetros ambientales. Materia orgánica disuelta coloreada, materia particulada en suspensión, clorofila a y blooms algales son los parámetros estudiados en este proyecto. Los resultados muestran el efecto de las tormentas ya que crean flujos terrestres masivos, así como la evolución de las concentraciones después de tales eventos. Para ello, los resultados se comparan con tablas meteorológicas. Se presenta la existencia de una correlación entre los parámetros (a excepción de los blooms). Además, demuestra el efecto que tiene un impacto humano repentino en un ecosistema que no ha sido perturbado durante meses.

Palabras clave: materia orgánica coloreada disuelta, materia particulada en suspensión, clorofila a, blooms algales, teledetección

Analysis of the evolution of sea water quality in the Spanish coast from satellite images before and during the quarantine caused by COVID-19

Resum:

Les imatges de satèl·lit són una forma de teledetecció que es pot utilitzar per a diversos fins ecològics. La teledetecció ha estat utilitzada fins i tot per analitzar la qualitat de l'aigua. Hi ha molts índexs que utilitzen els valors de diferents bandes per calcular paràmetres ambientals. Aquest TFM estudia l'efecte de la quarantena del COVID-19 a Espanya al Mar d'Alborán. En aquest assaig s'analitzen els canvis en la qualitat de l'aigua abans (des del 3 de febrer) i durant (fins al 22 de juny) la quarantena. Les dinàmiques estudiades són rellevants per a fins de restauració ambiental. Els índexs ja existents s'apliquen utilitzant ArcGIS i ACOLITE per determinar diversos paràmetres ambientals. Matèria orgànica dissolta acolorida, matèria particulada en suspensió, clorofil·la a i blooms algals són els paràmetres estudiats en aquest projecte. Els resultats mostren l'efecte de les tempestes ja que creen fluxos terrestres massius, així com l'evolució de les concentracions després d'aquests esdeveniments. Per això, els resultats son comparats amb taules meteorològiques. A més, es presenta l'existència d'una correlació entre els paràmetres (a excepció dels blooms). També es demostra l'efecte que té un impacte humà sobtat en un ecosistema que no ha estat pertorbat durant mesos.

Paraules clau: matèria orgànica dissolta acolorida, matèria particulada en suspensió, clorofil·la a, blooms algals, teledetecció

Acknowledgments

First and foremost, I would like to thank my tutors for guiding me through this experience. Lorena Parra Boronat, for suggesting the topic of this project and for answering my doubts when dealing with working with satellite imagery. And Jaime Lloret Mauri, for believing in me and guiding me through this step of my life. Both of them have helped me, and now I am more confident than ever that I want to do my PhD with Jaime's team.

I would like to express my gratitude to Jose Miguel Jimenez Herranz, without his help, this project would not have been done in time. He helped me by running the ACOLITE scripts and some of the ArcGIS indices on his computer, since it was faster than mine.

I would also like to thank my mother and father; without them I would not be here. My mother has always supported me and helped me relax when I got too nervous.

Finally, I would like to thank some of my friends, who supported me extraordinarily these months. Tomàs, since he helped me find the error when I ran into problems programming the ACOLITE scripts. Beato, for she listened patiently to me ranting about how long ArcGIS was taking to process the images. And last, but not least, Idoia, for being a spark of joy whenever I felt overwhelmed by this project.

Analysis of the evolution of sea water quality in the Spanish coast from satellite images before and during the quarantine caused by COVID-19

Index

Figures index

Analysis of the evolution of sea water quality in the Spanish coast from satellite images before and during the quarantine caused by COVID-19

Table index

1. Introduction

1.1. Introduction

This sub-section is divided in order to understand better the need for this project, as well as the current solutions to the problem, presented. Moreover, some interesting assets for the assessing of said problem are explained.

1.1.1. Motivation

The oceans and seas are crucial systems for most of the processes that occur on our planet. They not only serve as a source of resources (fishing, materials, energy...), but also as a location in which important socio-cultural activities are developed. Although they were once perceived as unchangeable, we are increasingly aware of how our actions affect the seas and oceans, making changes in them which can be irreversible.

When talking about environmental importance, non-continental water bodies are essential for life. Algae are an important resource in fixing carbon dioxide (CO2), which can be highly beneficial in stopping and reversing climate change [1]. If we focus on organisms, seas, and oceans have very high levels of biodiversity. Such biodiversity must be protected since it is already highly threatened right now [2].

The important sociocultural role of the seas and oceans must not be forgotten. During the last two centuries, the social viewpoint on coastal zones has changed. They used to be seen as unsanitary areas; now, they are seen as ideal vacation spots [3]. They serve not only as an idyllic place to spend free time and relax. Moreover, numerous recreational activities take place on the coast or in the sea, such as recreational fishing, surfing, regattas…

Tourism is one of the main economic activities on the coast, especially in areas with warm climates and clear sand beaches such as the Mediterranean and the Caribbean [4]. Not only is tourism economically important, but the oceans are also used daily to move goods across the planet. Moreover, they are sources of resources, such as fishing; and energy, such as tidal power or energy obtained from offshore wind farms.

For all these reasons, adequate protection of the seas and oceans is very important. Spill pollution, eutrophication, microplastics, are just some of the most pressing problems that plague our waters. Discharges can cause high mortality in a specific functional group or even several of them, as well as eutrophication problems.

Some toxins biomagnify, and can affect humans, as is the case with heavy metals such as mercury. But even nutrients can be harmful at high levels since they can generate algal blooms. This increase in microalgae produces eutrophication, causing a significant drop in the level of oxygen in an area [5]. Microplastics not only create problems in the ecosystem itself, but they can also bioaccumulate. They can even affect the metabolism of organisms since some plastics have endocrine disruptors [6]. There are many troublesome components we are letting go into seawater every day.

The need to follow these problems closely and to quantify their effects is clear. We, as the human race, have to do our best to avoid mistakes that have been made in the past, such as insufficient monitoring and incorrect management. Monitoring of environmental quality and detection of discharges is important when making the right decisions. Nevertheless, also, if we want to continue enjoying all the resources and activities linked to the seas and oceans, we have to ensure their good condition.

The study of the quality of seawater brings with it the problem of the devices used for measurements. The marine environment is aggressive; any instrument used on it is subject to salinity corrosion. The water in the various seas and oceans of Earth has relatively high salinity. Because of this, a sacrificial anode (usually zinc) should be used

on any instrument that requires long periods submerged [7]. Said salinity carries a conductivity that is in charge of the corrosion of any metallic element introduced into a marine environment. Nevertheless, this is not a problem when using satellite imagery.

Starting in March 2020, Spain went under emergency state due to the virus COVID-19. This situation, the virus, along with the quarantine, brought humankind many terrible things. Nevertheless, it also brought us the opportunity to study many environmental parameters when the human impact is minimum. With the ocean traffic almost stopped, the impact it had can be determined by comparing the data before and during the quarantine.

The quarantine began the 14th of March 2020 and was declared officially over, after several small steps (de-escalation), the 21st of June 2020. This is an event only preceded in our recent history by the Spanish flu. We can see the changes in the marine area brought by every step on the de-escalation in Figure 1. Moreover, Figure 2 presents the date in which every autonomous community entered every step of the de-escalation since it was not the same for all of Spain. These dissimilarities are due to the different sanitary situations they were going through.

Phase 0	Phase 1	Phase 2	Phase 3
Quarantine conditions	Exeptions in some Autonomic Communities for marine transport 50% ocupation with 2 meters between seats 100% ocupation in cabins for people living together	Recreational fishing allowed Recreational sailing only within the territorial unit	Passengers allowed to embark ferries Recreational sailing allowed within national territory

Figure 1: Effects of the de-escalation for the marine area [8]
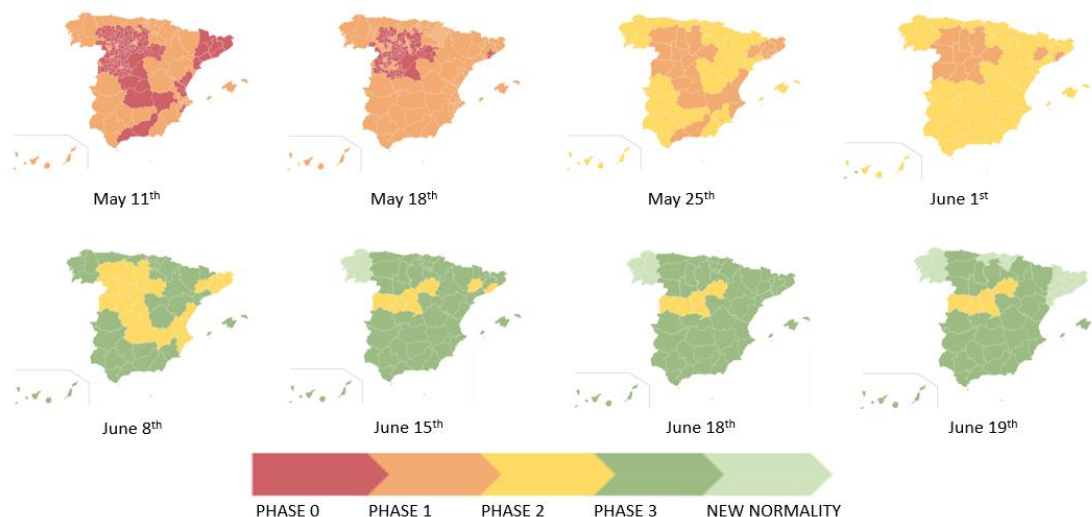
Figure 2: Time-lapse of the phases in Spain [9]

It is an amazing opportunity to study the behavior of some water parameters. The absence of traffic and the speculated decrease in pollutants from rivers is an unprecedented event in recent times. And as such, it should be studied.

1.1.2. Relevant parameters for seawater monitoring

When talking about seawater monitoring, there are several parameters which are worth studying. They can be divided between chemical, physical, biological, and

3

geological parameters [10]. The study of those four types of parameters is the backbone of adequate management of the water resources.

The type of marine organisms, as well as the density of the seawater, are determined by chemical parameters. They encompass pH, dissolved oxygen, salinity, and nitrogen, among others [11]. In order to establish the values for these parameters, either laboratory tests need to be carried out, or in-situ testing needs to be performed.

Physical parameters are vital in finding productive spots with high quantities of fish. Pressure, temperature, turbidity, density, and ocean currents are some physical parameters which affect seawater [12]. They are related to the energy interaction between the atmosphere and the ocean. The most used method to determine them is via satellite imagery and remote sensing.

The presence of algae, phytoplankton and zooplankton are the biological parameters [13]. Their study is essential in order to keep balance in marine ecosystems. Not only their presence or absence is important, but the nature of their metabolism is also part of their study. Optic methods are being used for their monitoring.

Among geological parameters, we find ocean depth, continental crust, sediment distribution, sea level and marine resources such as oil [14]. Ocean currents, seasonal changes, and swirls, as well as the presence of natural resources, depend on these parameters. Moreover, they must be studied before any structure is built near the shore. Nowadays, these parameters are studies using buoys (drifting, moored, Argo…).

The following table (Table 1) was done by Uma Kumari et al. [10] and represents the most commonly monitored ocean parameters, their range and the instruments and techniques used to measure them.

Table 1: Ocean parameters, their range and the instruments of techniques used to measure them [10]

Ocean parameters	Range	Instruments/Techniques
Temperature	-2 to 30 ºC	Platinum resistance thermometer, thermistors & quartz thermometers
Salinity	33.5–36.5 PSU	Chemical titration, inductive electrode & conductivity cells
Pressure	0–10000 dbar	Strain gauges, potentiometers, vibrating wire (Vibrotron), Bourdon tubes & quartz oscillators
Depth	0–10000 m	SONAR (echo sounder)
Density	1.03–1.07 g/cm^3	Thermosalinograph, vibrating tube densimeter & hydrostatic weighing.
Dissolved Oxygen	4–14 mg/lit	Iodometric method, Clark dissolved oxygen electrode and fluorescence quenching
pH	7.5–8.4	Electrode methods: Hydrogen electrode, quinhydron electrode, antimony electrode and glass electrode

The parameters chosen for this study are Colored Dissolved Organic Matter (CDOM), Suspended Particulate Matter (SPM), Chlorophyll a (Chl-a) and Harmful Algal Blooms (HABs). These parameters are relevant for several reasons.

CDOM [15] is the part of dissolved organic matter which can be detected via optical techniques. It is humic-rich and affects the light levels in the water column, therefore, affecting the entire ecosystem. It peaks naturally during spring and intense weather conditions such as storms and hurricanes. This is due to the fact that these events cause massive overland flows. Non-natural causes for peaks include human activities such as sewage treatment plant discharge and agricultural and farming runoff.

SPM [16] is linked to CDOM in due to both of them increasing with runoffs and both being sediments. It modifies the color and transparency of water as well. Nevertheless, SPM is associated with bacteria and metallic contaminants. Some human causes for an increase in the SPM levels include offshore wind farms, dams, sand extraction, transport of pollutants… Natural causes for SPM variation include water velocity and hydrological alternation [17]. Moreover, it can affect algal distribution.

Chl-a [18] indicates the trophic state of waters since it is a proxy for phytoplankton biomass. High Chl-a levels indicate eutrophication, a state for which dissolved oxygen becomes a scarce resource, thus affecting the entire ecosystem. This increase in phytoplankton happens when there is a high nutrient load. The Chl-a levels in the sea are usually lower than in lakes and coastal lagoons, nevertheless, they increase with weather events such as storms, for the same reason CDOM and SPM do. An increase in overland flow implies a nutrient load.

HABs [19] disrupt the entire marine ecosystem and can cause eutrophication. The frequency in which these phenomena have been showing has increased since the 1980s. They can impact the local economy, food security, human health and tourism. Climate change has been linked to blooms. The warming and acidification of the seas, as well as deoxygenation, all caused by climate change, increase the possibility of a HAB. Moreover, they can be caused by high nutrient loads after extreme climatic events such as storms or hurricanes.

1.1.3. Imaging techniques and sea monitoring

The oceans and seas are somewhat challenging to monitor. Nevertheless, imaging techniques offer a straightforward approach to the study of those areas. Some images, as well as some software for their processing, are even available for free. It is not a surprise to find a handful of indices which are currently being used for ocean and seawater monitoring. Even more, now that the information is available for the public [20].

There are indices and methods for the monitoring of many parameters, from more generic to more specific data [20]. Chl-a, SPM, turbidity and CDOM are examples of generic data. Whereas water depth, substrate mapping, particle size distribution and phytoplankton functional types are some more specific parameters.

There are bio-optical models which use the differences between the reflectance of different components which can be in the water and the water itself [20]. They get their name due to the things measured with these models being biological components. The absorbance, backscattering or reflectance of each component (and seawater) forms a spectral signature, which is a distinctive pattern used by bio-optical models to discern the components present on the image. Figure 3 [20] shows an example of absorption and backscattering for different components.
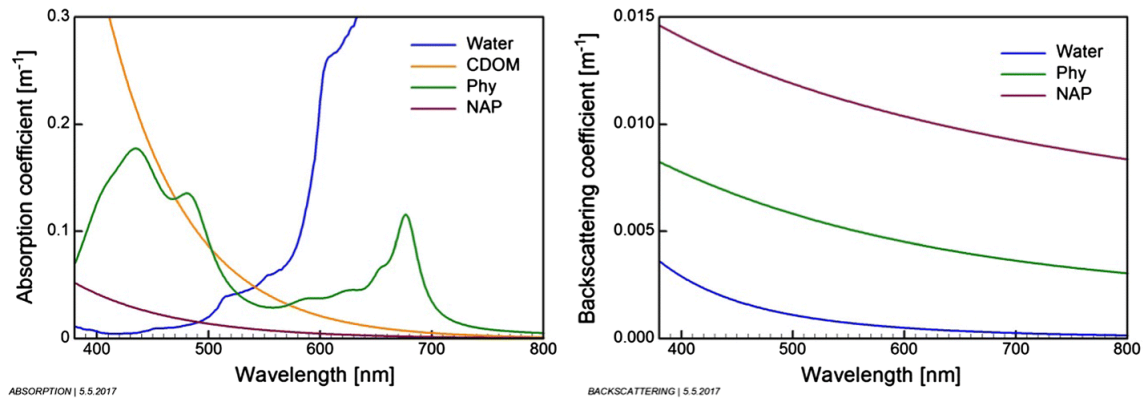
Figure 3: Examples of absorption (left) and backscattering (right) coefficients of water, CDOM, phytoplankton (Phy) and non-algal particles (NAP) [20]

1.1.4. Sentinel missions

The European Space Agency (ESA) launched, starting in April 2014, a series of satellites in order to monitor the Earth. Each satellite compromises an entire mission, they are named "Sentinel", and they were developed in conjunction with the European Commission initiative Global Monitoring for Environment and Security (GMES) [21].

The main objective is to ensure the data continuation by replacing the older Earth observation missions. Most of which have either reached retirement or are reaching the end of their life span. Several aspects of earth observation are covered with the missions: Oceanic, Land and Atmospheric monitoring. Moreover, these missions were developed within the Copernicus framework [22].

The missions were created with a collaborative mindset [23]. The data is available for free for anyone with a user account on the ESA webpage. Moreover, local ground stations can be set to receive Sentinel data almost at real-time during the satellite overpass. Furthermore, new tools and applications are being developed. Algorithms and products, which can include specific procedures for specific applications or regional coverage, are created and can be added to the Sentinel core product chains.
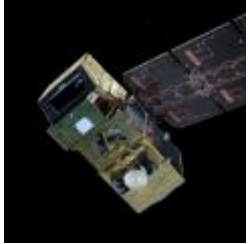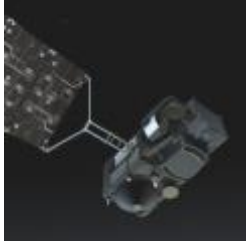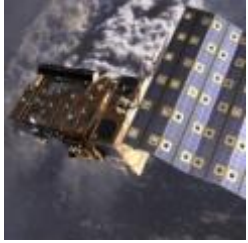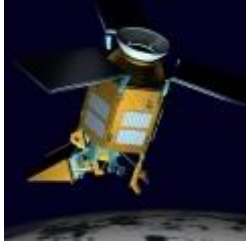
The missions focus on six thematic areas, which will be studied by the satellites. Among them, we find land monitoring, atmospheric monitoring, managing emergencies, security, climate change, and marine monitoring [24]. In this project, we will focus on the last one, marine monitoring. Table 2 shows the main characteristics of the different missions. Moreover, it shows a picture of each satellite. The information from Table 2 is available on the ESA webpage [21].

The mission used for this study, Sentinel-2, has a high revisit time due to the two satellites being phased 180 º. Furthermore, this mission covers latitudes from 56º S to 84º N. The two satellites which compromise this mission weight 1.2 tones and were launched with the European launcher VEGA. Their estimated lifespan is 7.25 years, although they were filled with enough propellant to fuel 12 years of the mission. It is endowed with a MultiSpectral Instrument (MSI) which collects the reflected sunlight, working passively. The products available to the public are the Level-1C, Level-1B and Level-2A images. Level-1C images are the ones which will be used in this study.

Although it was not created specifically for marine monitoring, the Sentinel-2 mission [25] offers high-resolution optical imagery. Therefore, the images from the satellites belonging to this mission are more suitable for imaging techniques. This is a crucial factor since, usually, the higher the resolution, the higher the price [26]. Nevertheless, Sentinel-2 offers high-quality imagery for free.

Analysis of the evolution of sea water quality in the Spanish coast from satellite images before and during the quarantine caused by COVID-19

Table 2: Sentinel missions overview

Mission	Satellites	Instruments	Objective	Picture
Sentinel-1	Two polar-orbiting satellites Operating day and night	Radar imaging	Land and Ocean monitoring Obtain imagery regardless of the weather	
Sentinel-2	Two polar-orbiting satellites	High-resolution optical imagery	Land monitoring Vegetation, soil, and coastal areas	
Sentinel-3	Three almost polar-orbiting satellites	Radar altimeter and optical imagers	Marine observation Sea-surface topography, sea and land surface temperature, ocean, and land color	
Sentinel-4	Two families of satellites: MTG-1 MTG-2 Geostationary orbit	Imager satellite Sounder satellite	Air quality Composition of the Earth's atmosphere Forecasting and monitoring over Europe	
Sentinel-5	On the MetOp-SG a polar-orbiting satellite	Spectrometer	Air quality Composition of the Earth's atmosphere All over the world	
Sentinel-5P	One satellite with a near-polar orbit	TROPOspheric Monitoring Instrument	Fill the data gap between the retirement of old missions and the Sentinel-5 (same monitoring as Sentinel-5)	

1.2. Objectives

The aim of this project is the study of the changes which happened in the Mediterranean coast in the Andalusia region during the quarantine caused by COVID-19. To compare them, satellite imagery will be used. These images will be from the satellite constellation Sentinel-2, more precisely using the Sentinel-2A treated images. Only one of the two satellites which compose the Sentinel-2 missions will be used in order to reduce the possible errors due to the possible dissimilarities between them.

It is also to be noted the study and determination of possible areas of interest, which could be more sensible to changes. Maybe the areas closer to ports and rivers since the contamination in them should be inferior to the contamination before the pandemic (fewer fabrics working). These areas could be of interest for a future study.

Moreover, the possibility of interpreting the data to create new management strategies is very interesting. The monitoring of these parameters could give key information to develop new routes for ships. In general terms, this type of study is unprecedented. Therefore, the possibilities of the information derived from it are very interesting.

In the recovery and restoration area of environmental sciences, it is very important to specify the state to which the environment should return. The standards to which the recovery is held are derived from either areas for which the human impact is reduced or areas which have already been restored. The data from the months after the beginning of quarantine show what would happen to a marine environment if all human activities stopped. Therefore, the results of this experience could be used for recovery and restoration purposes as well.

In this study, we present the comparison of several environmental parameters, such as CDOM, SPM, Chl-a and HABs before and during the COVID-19 quarantine in Spain. The objectives of this study are divided between Main Objectives (MO) and Secondary Objectives (SO). Following they are briefly described:

MO 1.: Determine, from satellite imagery, the environmental status of the Mediterranean coast in the Andalusia region before the COVID-19 quarantine.

SO 1.1.: Study the CDOM levels during that period.

SO 1.2.: Study the SPM levels during that period.

SO 1.3.: Study the Chl-a levels during that period.

SO 1.4.: Study the HAB which occurred during that period.

MO 2.: Determine, from satellite imagery, environmental status of the Mediterranean coast in the Andalusia region during the COVID-19 quarantine.

SO 2.1.: Study the CDOM levels during that period.

SO 2.2.: Study the SPM levels during that period.

SO 2.3.: Study the Chl-a levels during that period.

SO 2.4.: Study the HAB which occurred during that period.

MO 3.: Accurate portrayal of the changes which happened on this period.

SO 3.1.: Changes in the CDOM levels.

SO 3.2.: Changes in the SPM levels.

SO 3.3.: Changes in the Chl-a levels.

SO 3.4.: Changes in the HAB which occurred.

To do so, satellite imagery from the satellite Sentinel-2A will be used, as well as the software ArcGIS. The details of the process are further explained in Section 3.

1.3. Precedents at EPSG

Some works similar to the one presented in this study were found, although none of them seemed to measure several parameters. Soñes Bori [27] realized a study on the use of Sentinel-2 images to determine coastal bathymetry in 2019 in "COASTAL BATHYMETRY FROM SATELLITE HIGH RESOLUTION MONITORING".

Ruiz Fernandez et al. [28] wrote a book on satellite imaging, "TELEDETECCIÓN. NUEVAS PLATAFORMAS Y SENSORES APLICADOS A LA GESTIÓN DEL AGUA, LA AGRICULTURA Y EL MEDIO AMBIENTE" in which how remote sensing can be used for water monitoring is explained.

The use of remote sensing for the monitoring of the coastline is presented by Pintos Santos [29] in "ESTUDIO GEOMORFOLÓGICO EN LOS ENTORNOS COSTEROS CON MAREAS MEDIANTE LA EXTRACCIÓN AUTOMÁTICA DE LÍNEAS DE COSTA DE IMÁGENES DE SATÉLITE DE RESOLUCIÓN MEDIA".

Moreover, Tamburini et al. [30] discussed the use of satellite imagery for the detection of deep-sea bioluminescense blooms in "DEEP-SEA BIOLUMINESCENCE BLOOMS AFTER DENSE WATER FORMATION AT THE OCEAN SURFACE".

1.4. Structure

This project is structured as follows. Section 2 deals with some works related to the topic at hand. Monitoring done by Sentinel imagery (the one which will be used for this project), as well as monitoring done with imagery from other satellite constellations is described in said section. Afterwards, Section 3 describes the process through which the results will be obtained, focusing on the acquisition of the data, the pre-treatment, the main treatment, and the analysis. Next, the results and discussion are presented in Section 4. In this section, there are sub-sections for each parameter studied. Finally, Section 5 presents the conclusions, as well as some afterthoughts on the work done. Moreover, the possibilities for the future on this topic are presented in said section.
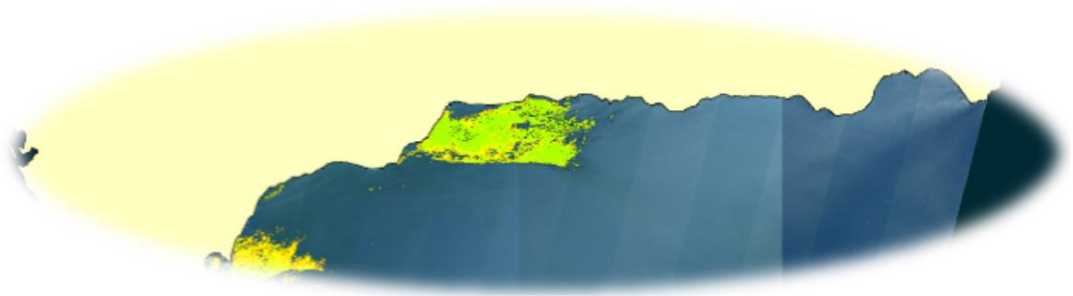
2. Related Literature

This section is divided into three sub-sections to improve the understanding thereof. The first sub-section explains some cases in which Sentinel imagery has been used to monitor environmental parameters, it focuses on those relative to the sea. The second sub-section shows a detailed report on Landsat-8 and Sentinel-2 possible combination and/or comparison. Moreover, the last sub-section explains how other satellite constellations are used to monitor parameters from the sea. All this information is submitted in order to further prove the importance of monitoring sea parameters as well as the usefulness of remote sensing for this purpose.

2.1. Monitoring by Sentinel-2

Toming et al. [31] proved the efficiency of Sentinel-2 MSI data for the monitoring of lake water quality at the global and local scale in 2016. They compared in-situ measures of CDOM, Chl-a and Dissolved Organic Carbon (DOC) with band ratio algorithms. They used both Level-1C (pre-treated) images and Level-2A images they atmospherically corrected using Sen2Cor. They employed the green to red band ratio to estimate the CDOM, DOC and water color. Chl-a concentrations were calculated using the 705 nm peak. They realized the atmospheric correction was reducing the band ratio algorithms correlation, thus indicating the need for better atmospheric correction. Nevertheless, the R^2 (a parameter which indicates the correlation from 0-no correlation to 1-perfect correlation) values from comparing the in-situ results with the calculated results were high for Chl-a, CDOM and DOC. They concluded that Sentinel-2 MSI data was going to be key in developing new water monitoring techniques and research.

Orlandi et al. [32] used imagery from the Sentinel-2 MSI sensor to map water quality indices. The bands used by them were visible and near-infrared, and they compared the results with in-situ data. They measured Chl-a, turbidity and total suspended solids (TSS) using fifteen images of the Pescara River estuary on the Adriatic Sea. The Level-1C images were run through two atmospheric correction programs, Sen2Cor and ACOLITE. The R^2 for the turbidity model was over 0.95. Although the R^2 for Chl-a was not the best, the model presented better results than the standard OC3 algorithm which was used before. They proved the usefulness of Sentinel-2 MSI data for coastal research and monitoring.

Caballero et al. [33] used Sentinel-2 imagery to monitor the southwestern Spanish coast. This experience was conducted during the first year Sentinel-2 imagery was available to the public. They collected in-situ samples of TSS in the Cadiz Bay, Guadalquivir estuary and Conil port. This was done to later compare the results derived from the model to the empiric results from the samples. They used an algorithm which selected the most sensitive TSS-water reflectance relationship to calculate the concentration. It used the red (664 nm) and near-infrared (865 nm) bands, both models presented high R^2 values. They used atmospheric correction strategies as well, ACOLITE and POLYMER. The latter proved to be quite useful for sun-glint effects. In conclusion, Sentinel-2 data turned out to be useful for TSS monitoring in medium to high turbidity waters.

Balasubramanian et al. [34] developed a model using Sentinel-2 imagery for the calculation of TSS concentrations. Their study is aimed at lakes, rivers, coastal waters and estuaries. In order to develop this model, they disposed of a large database of in-situ measures (over 3500 data). The bands used for the model were the red and near-infrared bands. Moreover, they used machine learning to improve the model. Since it is a Statistical, inherent Optical property-based, and muLti-conditional Inversion proceDure it was named SOLID. Not only was the model developed for Sentinel-2, but it was also tested on other missions as well. In conclusion, the results were good. Nevertheless,

there is room for improvement and for creating a model able to discern the type of particle.

Li et al. [35] were able to calculate SPM concentrations from the last twenty-two years using old imagery and a model created with Sentinel-2. First, they chose between five state-of-art models by comparing their results to 79 in-situ datasets from the estuary they were studying. The models were recalibrated as well, to ensure consistency. Then, they applied the chosen model to old Landsat imagery, from 1997 fo 2019. They were able to determine the SPM fluxes and, among other findings, discover seasonal patterns.

Liu et al. [36] used in-situ measures and Sentinel-2 MSI images to develop a model which could calculate the SPM concentration. The sixty-eight hyperspectral measurements they used were from Poyang Lake, China. Half of the samples were used to calibrate the model, whereas the rest of them were used to validate it. The resulting models were applied to new Sentinel-2 imagery and compared to the values from Terra-Moderate Resolution Imaging Spectroradiometer (MODIS) B1. The models, which used bands 4 to 8A proved to explain 77-93 % of the SPM concentration variation. The most accurate models were the ones which used band 7 for high loadings of SPM and band 4 for low loadings.

Saberioon et al. [37] developed a semi-empirical model using Sentinel-2 data and samples from several water reservoirs. They used machine learning to improve their model, using up to ten spectral bands and nineteen spectral indices. The models had to be able to calculate Chl-a and TSS concentration. The end models had R^2 values over 0.8 and performed better for higher concentrations. They were able to show spatiotemporal changes. In conclusion, Sentinel-2 imagery could be combined with machine learning algorithms for a low-cost, reliable and accurate monitoring instrument.

Hafeez et al. [38] USED Sentinel-2 MSI red bands to monitor Chl-a and TSS concentrations in the Pearl River Estuary and the coastal waters of Hong Kong. They used the red band algorithm and Case-2 Regional/Coast Colour C2RCC. The later was used for atmospheric correction. They managed to monitor them, along with red tide blooms with high concentrations of TSS. The methods used showed R^2 values over 0.7.

Potes et al. [39] tested previous algorithms developed for the ENVISAT-1 with Sentinel-2 data. The area of study they chose was the Alqueva reservoir, Portugal. Moreover, they rested the effectiveness of the algorithms for the new MSI instrument for Chl-a, water turbidity, density and concentration of cyanobacteria. Their results were compared to in-situ sampling and the analysis of Chl-a associated with HAB in laboratories. The MSI sensor was able to detect HAB.

Ha et al. [40] studied the use of Sentinel-2 imagery for the estimation of Chl-a concentration in Lake Ba Be, Northern Vietnam. The study site is a Ramsar site, as well as being the largest natural lake in Vietnam. The model developed in their study was compared to data from thirty surveyed sites around the lake. For the model, they used green-red band ratio (bands 3 and 4). The R^2 value of the model was almost 0.7, proving to be an interesting tool for the monitoring of Chl-a concentrations in water.

Khalili et al. [41] tested up to fifteen different indices for the HAB monitoring using Sentinel-2 MSI data. Specifically, the tests they performed were aimed at the detection of red tide algal blooms. For each index, different statistical parameters were calculated such as overall accuracy, type I and II error, area under the curve and Kappa coefficient. The model which presented the best results taking into account the statistical parameters was (band4–band8A)/(band4+band8A).

Alba et al. [42] used Sentinel-2 imagery to monitor an algal bloom event. This event occurred in Sna Roque lake, Córdoba, Argentina. The bands used to detect the HAB were bands 4 and 8. Moreover, they used bands 8a and 9 to discern the algae composition patterns. The results were positive and showed the potential Sentinel-2 MSI data has for the monitoring of bloom events in eutrophic lakes.

2.2. Comparing Sentinel-2 and Landsat-8

Pahlevanet al. [43] tested the MSI data processing using the SeaWiFS Data Analysis System to monitor aquatic systems. They compared the resultant reflectance products derived from the Sentinel-2 imagery from those obtained from Landsat-8. Landsat-8 is endowed with an Operational Land Imager (OLI). Their comparison was made using in-situ water-leaving radiances. They proved the blue and green bands present an insignificant error between the MSI imagery, OLI imagery and in-situ data. Moreover, they used the MSI imagery to calculate a TSS through a time frame for an inland system. Furthermore, they noted the need for an improvement in the atmospheric correction in water bodies with high dissolved organic matter or suspended particles concentrations. Better mitigation of the haze at low solar zenith angles was needed as well as a minimization of image artifacts.

Bande et al. [44] used both Sentinel-2 and Landsat-8 data to monitor the water quality at Vaal Dam, South Africa. They wanted to test whether Sentinel-2 would yield better or worse results than Landsat-8. The parameters they calculated using imagery from both satellite missions were turbidity and Chl-a. After comparing with in-situ measures, the best results were those generated by Sentinel-2 imagery. The R^2 values for both parameters were higher for the results derived from Sentinel-2 data.

Pahlevan et al. [45] compared more parameters for Sentinel-2 and Landsat-8. Such parameters include top-of-atmosphere reflectance, biogeochemical properties (TSS among them) and remote-sensing reflectance. The areas of study encompassed many highly turbid/eutrophic inland/nearshore waters. The differences found were less than 5% of the total for the remote-sensing reflectance. Later TSS tests confirmed this. The need for a better atmospheric correction procedure was shown by some negative retrievals of remote-sensing reflectance. Nevertheless, the utility of combining Sentinel-2 and Landsat-8 imagery for water monitoring was proved.

Peterson et al. [46] combined Sentinel-2 and Landsat-8 imagery to monitor several water parameters. Using deep learning methods, they managed to estimate blue-green algae, Chl a, dissolved oxygen, fluorescent dissolved organic matter, turbidity, and specific conductance. After applying the newfound models, the R^2 values obtained were higher than 0.84 for all the tested parameters.

Caballero et al. [47] used both Landsat-8 and Sentinel-2 imagery to monitor the TSS in the southwestern Iberian Peninsula. The areas of study were the Cadiz Bay and the Guadalquivir estuary. They were able to detect turbidity plumes and proved the effectiveness of fusing both missions. Said merging resulted in a higher frequency of measures, which translates into better monitoring. This is especially convenient in latitudes prone to being covered by clouds.

Xu et al. [48] used CDOM absorption spectra parameters to create an index to calculate its concentrations on a lake from satellite imagery. They used Sentinel-2 and Landsat-8 imagery for this experiment. The 92 different samples were taken for two years (2015-2016) in four different study areas. The models performed better when the threshold of concentration was set as 10 mg/L. They concluded that the results from the

models run on Sentinel-2 were more accurate than those from the models run on Landsat-8. The best band ratios for Sentinel-2 were B4/B2, B5/B2, B7/B8 and B7/B8A.

Both Cao et al. [49] and Chen et al. [50] used Sentinel-2 and Landsat-8 to monitor CDOM and DOC. They used similar methodologies to generate new models and validate them. Moreover, both teams concluded that Landsat-8 and Sentienl-2 imagery could be combined for better monitoring. Both satellites generate similar data. Nonetheless, Sentinel-2 has a higher resolution.

2.3. Other missions and satellites

Kostianoy et al. [51] tested the ability of several satellite remote sensing constellations to monitor the environmental status of the Boka Kotorska Bay, Montenegro. They used data from SPOT, Landsat, Radarsat-2, FORMOSAT-2, QuickBird, Sentinel-2A and Sentinel-1A, among others. All the images used had a high spatial resolution. They were used to monitor Chl-a, turbidity, sea surface temperature and roughness. Moreover, they were able to detect forest fires.

Ogashawara et al. [52] used the Sentinel-3 Ocean and Land Colour Instrument (OLCI) for the monitoring of cyanobacterial HABs. They did this by detecting the pigments Chl-a and phycocyanin. The area studied was the western part of Lake Erie, USA. They used single, and band ratios to estimate the pigments and found strong correlations. Thus, proving the usefulness of Sentinel-3 imagery to estimate cyanobacterial HABs.

Khan et al. [53] studied the relationship between Chl-a and sea surface temperature using data obtained from Terra-MODIS. The imagery used in their experience is from the time-period from 2001 to 2017. Using the Data Interpolating Empirical Orthogonal Functions (DINEOF) method, they were able to enhance the data. Moreover, they were able to check the correlation between Chl-a and sea surface temperature over the Persian Gulf and certain parts of the Arabian Sea.

Benallal et al. [54] used imaging from MODIS Aqua, among other parameters, to monitor the air-sea CO_2 flux. The sea surface temperature, Chl-a, sea surface salinity and seawater CO_2 fugacity were estimated from the MODIS Aqua imagery. Other parameters used include wind speed and atmospheric CO_2 fugacity. The results calculated from the satellite data were compared to in-situ data for the calibration of the model. Overall, the model was a success.

Schaeffer et al. [55] tested the potential of Landsat-5 and Landsat-7 for the monitoring of surface temperature in lakes. They used temperature data from the thermal band products from the U.S. Geological Survey Landsat 5 Thematic Mapper and Landsat 7 Enhanced Thematic Mapper Plus. They were validated across twenty-four estuaries and thirty-five lakes and reservoir. In order to do so, in-situ data was used. This study proved the possibility of using Landsat data, which compromises over thirty-five years, instead of in-situ data.
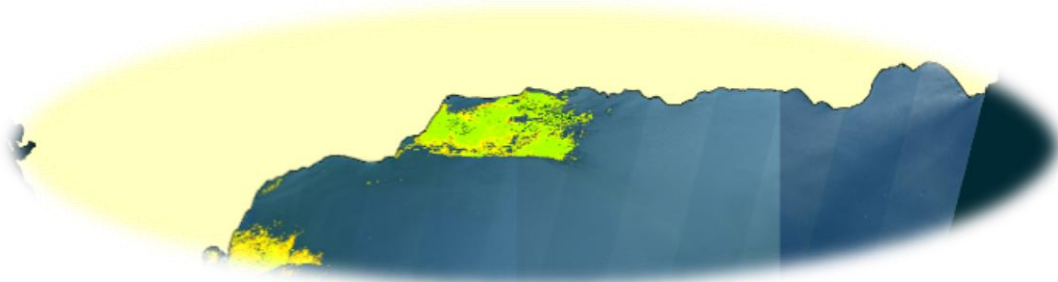
3. Test Bench

This section is divided in in four sub-sections, some of them with sections as well. This structure is done to ensure a better understanding of the process through which the results will be obtained. First, the method used to obtain the data is shown. Afterwards, the process through which said data would be treated before applying the indexes is thoroughly explained. Moreover, those indexes are explained, as well as the ArcGIS Tool used to obtain the results. Finally, a brief description of the criteria used to determine the changes is exposed.

3.1. Data acquisition and management

The data used for this project will be extracted from the Copernicus Open Access Hub [56]. In order to do so, the first step is to create an account in the said webpage. Once the user has an account, data from all over the world can be accessed, from every Sentinel satellite, for free. The webpage has an interface in which the user can select the time-period, the area and the type of image they want. Once selected, a download is started, and the user gets .zip files, which need to be decompressed.

Once decompressed, between folders of metadata, 14 .jp2 files can be found. They can be read as rasters by ArcGIS. Those files are stored inside the folder names "GRANULE", inside a folder in the folder "IMG_DATA". The two folders specified are always named the same, whereas the names of the other folders depend on the date and area of the image. The files found on the "IMG_DATA" folder correspond to the different bands. These are rasters for which the value of the pixel is the reflectance at different wavelengths. Said wavelengths, as well as what they depict and their resolution (pixel size), are noted in Table 3.

Table 3: Description of the .jp2 images obtained

Band name	Wavelength (nm)	Description	Resolution (m)
B01	0.443	Coastal aerosol	60
B02	0.490	Blue	10
B03	0.560	Green	10
B04	0.665	Red	10
B05	0.705	Vegetation Red Edge	20
B06	0.740	Vegetation Red Edge	20
B07	0.783	Vegetation Red Edge	20
B08	0.842	Near Infrared (NIR)	10
B8A	0.865	Vegetation Red Edge	20
B09	0.945	Water vapor	60
B10	1.375	Short Wave Infrared (SWIR) - Cirrus	60
B11	1.610	SWIR	20
B12	2.190	SWIR	20
TCI	-------	True Color Image	10

Taking into account the nature of the images used for this study, Sentinel-2A divides the Andalusian Mediterranean coast in four. These sub-areas are determined by Sentinel and will be selected in order to ensure the presence of data from all the Alboran coastline. The names of the sub-areas are marked with three letters, for this study the sub-areas selected are STF, SUF, SVF, and SWF

This area was chosen due to the usually high marine trafficking present on it. It is the metaphoric door to the Mediterranean Sea, the Strait of Gibraltar. Every ship

coming from outside the Mediterranean Sea, destined to a port in it has to go through the Alboran sea. Therefore, it is a suitable area for the study of possible changes due to the COVID-19 quarantine.

As stated before, there are four sub-areas, each corresponding to different parts of the Alboran sea. Figure 4 shows the days for which we have data, taking into account the fact that the first day from which we have data is the 3rd of February. Moreover, we know Sentinel-2A has a return time of 10 days in this area.
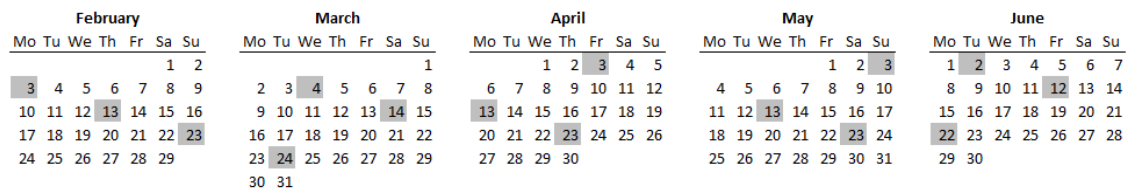

Figure 4: Days for which there are data

Therefore, the last datum for the area of interest corresponds to the 22nd of June, barely a day after quarantine finished. This makes a total of fifteen days, an average of three per month, of data.

The sub-area SWF has data for more days than the those studied for this project. This is due to the fact that this sub-area is in the limit between two runs from the satellite. Therefore, there are days we will not use from this sub-area, due to the fact that there is only data for it and not for the others.

In order to keep the data organized and tracked, they will be stored in folders per day and per month. Thus, having five folders (February, March, April, May and June) with three folders inside (one per day) containing the four folders (one per sub-area) downloaded from the Copernicus Open Access Hub [56].

## 3.2. Data treatment
3.2.1. Pre-treatment

The images which will be used for this experiment are Level-1C images. This means they have already undergone a pre-processing before they are accessible to the public [57]. This process includes geometric and radiometric corrections with both spatial registrations and ortho-rectification. The global reference system ensures sub-pixel accuracy. This step is not further explained in this section since it will not be done by the student.

Therefore, the images obtained from the Sentinel webpage will have already been through the above-mentioned pre-treatment. Nevertheless, they will need to be further processed before some of the indices are calculated.

The software ACOLITE [58] will be used for this step. This software can process Sentinel-2 (A/B) and Landsat (5/7/8) imagery and was developed specifically for inland water and coastal applications. Among the processes it performs, the most important is the atmospheric correction; this is done using the dark spectrum fitting approach [59]. Moreover, it can apply indexes and existing formulas to derive parameters with their corresponding values. This software has been proved to be useful for Sentinel-2 before [60].

When ACOLITE is installed on a computer, three folders can be found inside the program folder. The "config" folder has several .txt files. One of them is named "acolite_defaults.txt" which has the settings of the program. Those settings can be changed creating a new .txt file with the new settings. Currently, it works with Python 20190326.0. When running the program two windows appear on screen, one of them

only shows the processes the program is going under. The interesting window is the other one, and Figure 5 shows the default settings on that window.
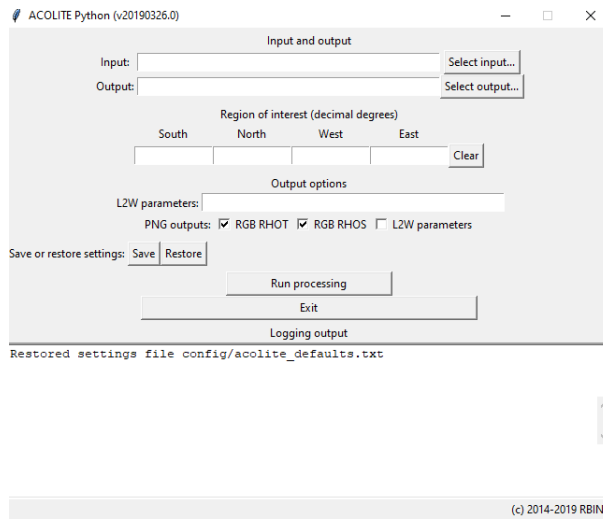
Figure 5: ACOLITE window with default settings

The Logging output informs the user of the current settings, which are, by default, the ones specified in "acolite_defaults.txt". They can be changed by clicking on the Restore button. A window opens, and a new file can be chosen to change the settings. The scripts need to be saved as .txt files in order to be run by ACOLITE. The changes can be seen in the same window, and Figure 6 shows the line in Logging output which informs about the new settings, as well as the changes.
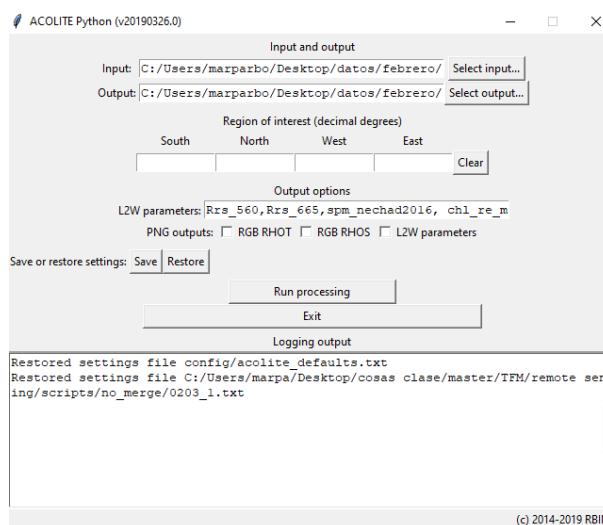
Figure 6: ACOLITE window with new settings

The only step left for the ACOLITE treatment is to click on "Run processing" and wait for the images to be generated on the specified folder.

It is to be noted that part of the main treatment will be applied when running the scripts, more specifically, for the Chl-a and SPM indices. Nevertheless, this step is just the beginning for the HAB and CDOM indices.

Although ACOLITE can represent HAB, the index used in this study is different. The first step for the pre-treatment of the images used for the HAB index is to merge the images for B4 and B8A. This will be done using the ArcGIS software [61], more precisely the "Mosaic To New Raster" tool [62], which can be found in the Data Management Tools.

To use this tool, the different rasters are uploaded, the output folder is determined, and the name of the new raster is set, as well as the extension. In this case, it will be opted to use the format .tif for the new rasters. Moreover, the type of pixel has to be established, which will be chosen to be "16 bit unsigned" in order to be able to have values from 0 to 65535. The Coordinate System will not need to be described as it takes the coordinate system from the first original raster as the coordinate system for the result. The number of bands has to be specified as well; in this case, it will be one.

Moreover, the "Mosaic Operator" will be set to "Mean". This indicates which value to take for the places where sub-areas overlap since for our area none of the places where the sub-areas overlap has no data, "Mean" is the best option. Finally, it does not matter what will be chosen for "Mosaic Colormap Mode", since all rasters share the same colormap (black for values close to 0 to white for higher values). The final setting for the "Mosaic To New Raster" tool for our area can be seen in Figure 7. After entering all the data and selecting all the options, all is left will be pressing run.
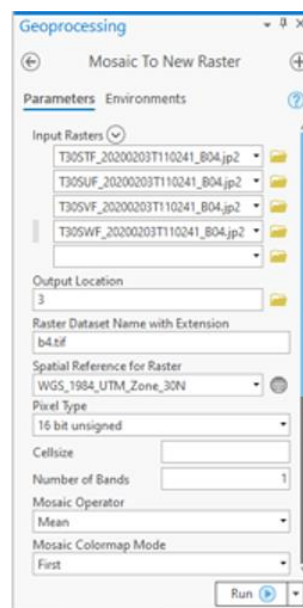
Figure 7: Mosaic To New Raster for the area

This will be done two times for each day: one for B4 and another for B8A. It is to be noted that B8A has a smaller resolution than B4; therefore, it is expected for the process to take less time for B8A. When finishing there should be a total of thirty images, two per day.

Those images are the ones which will be used later for the main treatment for HAB. Said treatment is explained with detail in the next sub-section.

3.2.2. Main treatment

The ACOLITE script for each day is a modification of "acolite_default.txt" to which new commands will be added and some old commands will be modified. The input and output will be selected, as well as the 12w parameters (among them, the indices). Moreover, it will be specified for the results to be obtained in .tif format and to not generate .png files. One of the full scripts can be seen in Annex I, the changes applied are these:

```
## Input the file from the correspondent folder

inputfile=C:/Users/maparbo/Desktop/datos/febrero/3/S2A_MSIL1C_20
200203T110241_N0208_R094_T30STF_20200203T113113.SAFE
```

```
## Chose the output folder

output=C:/Users/maparbo/Desktop/datos/febrero/3/S2A_MSIL1C_20200
203T110241_N0208_R094_T30STF_20200203T113113.SAFE

## output l2w parameters

l2w_parameters=Rrs_560,Rrs_665,spm_nechad2016, chl_re_moses3b740

# output RGB / L2W maps

rgb_rhot=False

rgb_rhos=False

map_l2w=False

# GeoTIFF export options

l2r_export_geotiff=False

l2w_export_geotiff=True
```

The Rrs_560 and Rrs_665 images will be used for the CDOM index, and before calculating it, it will be needed to combine them. This will be done following the same method as for the HAB images, combining the B3 and B4 images in this case.

The main treatment for the Chl-a and SPM will be done by ACOLITE and the files generated by spm_nechad2016 and chl_re_moses3b740 will be ready to be analyzed. For the main treatment for HAB and CDOM another ArcGIS Tool will be used. In this case, the chosen Tool is one which is useful for many remote sensing applications; it is the "Raster Calculator" [63].

Rasters can be interpreted as large matrices in which each pixel is one number from the matrix. With this in mind, the Raster Calculator operates as, according to its name, a calculator for matrices. It applies a specified formula to the matrix represented by the raster, said formula is entered in the section below the section where rasters are entered. It has to be filled with rasters from the "Rasters" section and Operators from the "Tools" section. The rasters can either be entered manually clicking on the folder icon next to the section or are automatically displayed on the section when they are on the map. The name and extension for the output raster have to be specified as well. The empty setting of the tool can be seen in Figure 8.
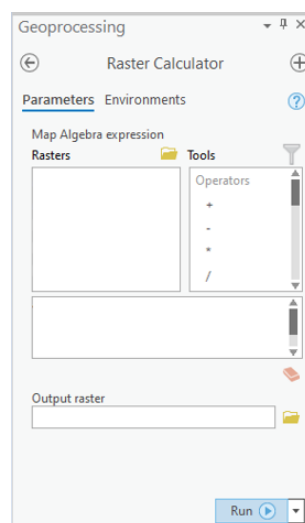
Figure 8: Raster Calculator tool

Several indices, explained in the following sub-section, will be used. They will be calculated using this tool.

3.3. Used indices

In this sub-section, the indices used to estimate the levels of CDOM, SPM, Chl-a and HAB are described. To ease the understanding, thereof this sub-section has been divided into four brief parts. Each of them deals with one of the indices. The first one explains the CDOM index. Next, the SPM index is shown. Afterwards, the Chl-a index is presented. Finally, the HAB index is explained.

3.3.1. Colored dissolved organic matter (CDOM)

The index used for the CDOM is derived from the studies conducted by Chen et al. [45]. They determined the formula to estimate the CDOM levels using the bands 3 and 4. Said formula can be seen in Eq 1. Moreover, the complete setting of the Raster Calculator tool [63] is shown in Figure 9. It is to be noted the fact that the output raster will be saved on the folder containing the information from that day.

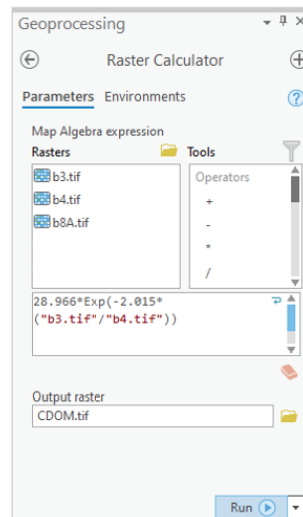$$28.966 \cdot e^{-2.015 \cdot \frac{B3}{B4}} \tag{Eq. 1}$$

Figure 9: Raster Calculator setting for the CDOM index

The results from this equation will be the CDOM concentrations in mg/L for each pixel. It is to be noted that each pixel will be 10x10 meters in real life due to the fact that both images used for this index have that resolution.

3.3.2. Suspended particulate matter (SPM)

The SPM levels will be derived from the rasters generated by ACOLITE. The program will use the formula developed by Nechad et al. [64]. First, it will apply an atmospheric correction to the images, next using the NIR images, the concentration (in g/m^3) will be calculated for each pixel.

This step will be done when running the script on ACOLITE, and there is no need for the use of ArcGIS to generate this data, only to display it.

3.3.3. Chlorophyll a (Chl-a)

In the case of Chl-a, the results will be obtained from ACOLITE as well. The formula used is from Moses et al. [65]. Said formula usually employs 780 nm as a reference. Nevertheless, it can be specified for it to use 740 nm. This was chosen due to the concentrations being slightly higher when employing the 740 nm band as

reference. When determining harmful concentrations, it is better to overestimate them. Moreover, since the objective is to compare the changes between different days, it is better to have higher values, the changes can be more notable.

The concentration will be calculated for each pixel and will be shown in µg/L. The treatment will be conducted by ACOLITE during the pre-treatment. ArcGIS will only be used to display the data.

3.3.4. Harmful algal blooms (HABs)

For Chl-a the formula used will be the one determined to be the best for this type of measures by Khalili et al. [41]. This formula, Eq. 2, is different from the ones for the indices above. It is a division which shows the pixels that have a higher difference between the bands for Red and Vegetation Red Edge. It is to be noted that the B8A band has a smaller resolution than the B4 band. Therefore, their result will have the smallest resolution out of them (20 m). It will be done using the Raster Calculator Tool [63]. The setting for it can be seen in Figure 10.

$$\frac{B4 - B8A}{B4 + B8A} \qquad \text{(Eq. 2)}$$
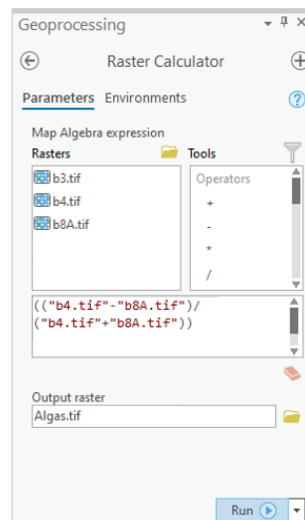
Figure 10: Raster Calculator setting for the HAB index

The results for this index will range from -1 to +1 due to the nature of its equation. For pixels where the value for B4 is significantly bigger than for B8A the result will be close to 1. Whereas for pixels where the value for B8A is significantly bigger than for B4 the resulting pixel will be close to -1. In pixels where the values for B4 and B8A are similar, the resulting pixel will have a value close to 0.

According to Khalili et al. [41] HAB laden waters present bigger differences for B4 and B8 than normal seawater. Therefore, values closer to 1 will be HABs, whereas positive values closer to 0 will be water. Clouds are white; therefore, the reflectance for B4 and B8A is similar for them. It is to be expected that numbers close to 0 are clouds. Positive values are ground; nevertheless, in this essay, that is not being studied.

3.4. Analysis

The resulting images will be displayed using ArcGIS. Using their pixel values to color the images, four results will be obtained per day. The CDOM, SPM and Chl-a values will correspond to their concentrations, whereas the HAB values will have to do with the presence or absence of them.

For the study of CDOM, the values range from 0 mg/L (water) to around 30 mg/L for some areas during storm periods. Nevertheless, most of the days only have values up to 8 mg/L. Therefore, a color will be assigned every 2 mg/l up to 8 mg/L, paying closer attention to these concentrations since they are the usual ones. For concentrations higher than 8 mg/L, only two distinctions will be made. Concentrations from 8 mg/L to 15 mg/L and from 15 mg/L to 30 mg/L. Although it is unusual to pay less attention to higher concentrations, these happen during storm periods, and they are not the values during normal circumstances, which are what we are attempting to study. The colors assigned to the concentrations will be green for lower concentrations, then yellow, orange, red, pink, and purple.

For the SPM concentrations, it is to be noted that concentrations from 0 to 2 g/m^3 correspond to the sea. The rest of the concentrations will be ranged every 4 g/m^3. This will be done up to 18 g/m^3. The colors used for this index indicate the concentrations as well, using green and yellow for lower concentrations and red for higher concentrations.

In the case of Chl-a, the concentration is in µg/L. They range from 0 µg/L (water) to around 100 µg/L, with some peaks over 1000 µg/L but lower than 2000 µg/L. They will be divided into seven intervals. The first interval will be 0 µg/L or less, to rule out water. Then, four intervals containing 25 µg/L each, until 100 µg/L. Finally, an interval from 100 µg/L to 1000 µg/L and an interval from 1000 µg/L to 2000 µg/L. Values over 2000 µg/L are most likely errors due to the images not lining up perfectly. Similar to the CDOM, the attention is centered around values lower than 100 µg/L due to them encompassing most of the values. The color will indicate the concentrations, red for higher concentrations and green for lower concentrations, with yellow and orange as intermedium concentrations.

For all these three indexes the values corresponding to the sea will be represented in blue, and their transparency will be turned up to an 80%. This will be done in order to represent underneath the true color images. These images will place the clouds and help interpret the results.

Finally, HABs will be monitored in this essay through distribution, not concentration. Since this index can differentiate sea, clouds and HABs, that is the distinction which will be used for the index. Values lower than 0,1 will be represented in white to show the cloud distribution. Since the study area is water, there is no need to assign a color to positive values for the earth. Values from 0,1 to 0,4 will be represented in blue, for water. Finally, values over 0,4 will be represented in red, for HABs. This is the only index in which the true color images will not be represented.

It is important to note that the SPM and CDOM concentration levels (measured in mg/L and g/m^3 respectively) can be considered equivalent due to the seawater density being close to 1,00 g/cm^3. Nevertheless, the Chl-a concentration levels, in µg/L, presents a difference in concentration values one thousand times smaller than the other two. This is due to Chl-a levels being very low at sea.

In order to make sure it rained whenever clouds are present in the pictures, weather tables [66] will be checked. A summary containing the information from tables is presented in Annex II. The values do not represent the magnitude of the storm at sea though. Nevertheless, they can assert the presence of rain.
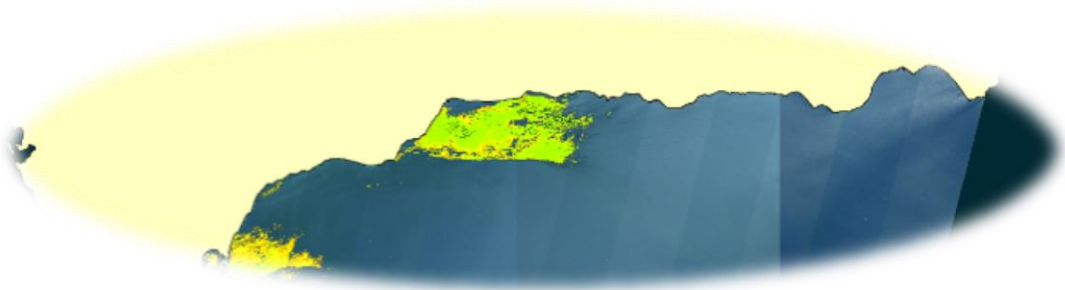
4. Results and discussion

This section presents the results for each of the parameters monitored in the area and time-period specified for this study. To better understand them and to achieve a clean presentation of the results, this section has been divided into four subsections. The first one deals with the changes in CDOM. Next, the evolution in SPM is presented. Moreover, the spatial-temporal changes in Chl-a are shown in the third sub-section. Next, the distribution of HAB is presented in the fourth sub-section. Finally, a summary of the changes is presented.

In order to improve the use of space, each month has been represented in one figure which contains three images, one for each day of the month. Each figure will occupy a page in which the description and explanation of the results shown in the said figure will be shown.

The images are labeled a), b) and c). The images corresponding to the first studied day of the month are represented as a). Next, the images which display the results for the second studied day of the month are labeled as b). Finally, the images showing the concentrations for the third studied day of the month are those marked as c). The days for each month and their label can be seen in Table 4.

Table 4: Arrangement of the days per figure

	a)	b)	c)
February	3rd	13th	23rd
March	4th	14th	24th
April	4th	14th	24th
May	3rd	13th	23rd
June	2nd	12th	22nd

The scale, as well as the north arrow and a legend, are present in all the figures. The scale for all the images is the same, 1:1000000. Moreover, it is displayed both numerically and graphically. The north arrow is almost pointing upwards since the traditional representation of Spain already has the north on top.

The legend for each figure shows the units in which the parameter studied in the said figure has been measured. Moreover, the colors representing the different ranges, which are explained in sub-section 3.4., are displayed. This assures an easy and very visual understanding of the results.

It is to be noted that the time-period studied in this project was very cloudy, which is to be expected from a winter-spring time interval. This is shown in the pictures since half of them show clouds. Moreover, for five of the dates studied the study area is almost fully covered by clouds. Nevertheless, the images have been thoroughly studied, and the results derived from them are presented in this section, broken down for an easier understanding.

4.1. Colored dissolved organic matter (CDOM)

In this sub-section, the results concerning the concentrations of CDOM are presented. As stated before, CDOM is an important parameter for the environmental monitoring of water. Taking into account the time-period presented in this essay, an increasing is to be expected.
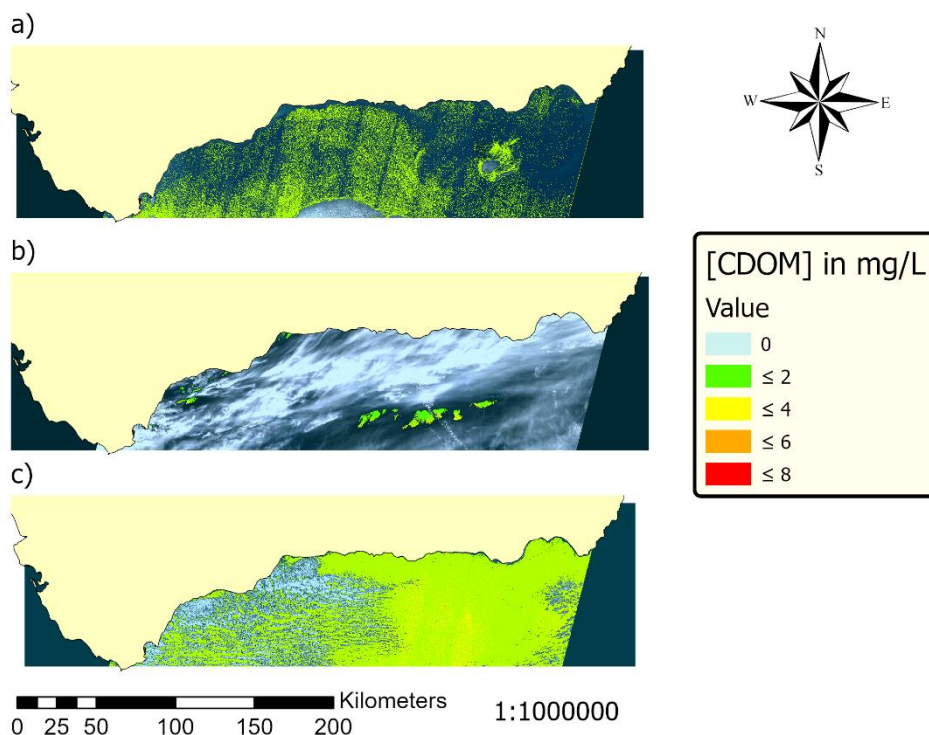
The CDOM concentration levels for the month of February are presented in Figure 11. The first thing which can be appreciated in the said figure is the storm covering the second day (11b), the 13th. There are clouds on all three days. Nevertheless, those clouds are small and localized for the first day (11a), the 3rd. For the third day (11c), the 23rd, they only cover the western part of the Alboran Sea.

Most values on February 3rd show concentrations lower than 2 mg/L. Their distribution does not seem to reveal any pattern other than it being slightly more prominent near the clouds. This could easily be an error due to dispersed pixels from the cloud being accounted as water pixels and thus processed by ACOLITE. It is important to note that these concentrations correspond to data taken in the middle of winter and before the quarantine started. Natural CDOM peaks usually happen during spring [15].

For February 13th the results are more difficult to interpret since there were many clouds. Nevertheless, the data shown on the gaps between clouds present higher concentrations of CDOM. The concentrations for those areas, higher than that of the 3rd, can be explained through the small storm that had been going on as seen in the weather tables from [66].

Even though some clouds are present on February 23rd, most of the data can be interpreted. An overall increase respecting the concentrations from February 3rd can be seen. Concentrations from 2 mg/L to 4 mg/L can be found in the southeastern part of the area. This can be correlated with the storm which happened during the week before. Moreover, this date is closer to spring, which is the season in which CDOM peaks naturally happen [15].

Overall, we can see an increase in the CDOM concentrations in the Alboran Sea during this month. This is most likely caused due to the storms discharging rain, which, in turn, created massive overland flows.

Figure 11: CDOM concentrations for February for which each map represents a) February 3rd, b) February 13th and c) February 23rd

For the month of March, the CDOM concentration levels are presented in Figure 12. For the first day (12a), March 4th, the sky is clear. Nevertheless, for the second day (12b), March 14th, clouds cover the western part of the Alboran Sea in a similar way to the image from February 23rd. Finally, for the third day (12c), Mach 24th, the sky is almost fully covered, even though the eastern part of the sea seems visible, it is covered by thin clouds which difficult the imaging techniques.

The values from March 4th show concentrations from the 0 mg/L to 2 mg/L range and from the 2 mg/L to 4 mg/L range. The distribution shown by them is similar to the one present on February 23rd (Figure 11c). This could easily be explained due to the rains experienced the week before, as seen in the weather tables [66]. The conditions already present ten days before are maintained.

According to the weather tables [66] heavy rains hit the peninsula the week before March 14th, the date in which quarantine started. Moreover, there are some clouds which only allow the eastern part of the Alboran Sea and the coastline to be studied on this date. The storms would explain the increase in concentrations. Some parts of the sea present concentration values over 4 mg/L. Furthermore, there seems to be higher concentrations nearshore. This could be explained if the satellite image was taken right after a storm, when the overland flow is still close to the shore.

For March 24th not much can be analyzed since clouds cover most of the sea. The CDOM concentration peaked, reaching values of even 8 mg/L. This can be explained due to the intense weather conditions that week, which created massive overflows and then the currents pulled the matter together in one point/direction.

This month, in which spring and the quarantine started, is dominated by changes due to the rain.
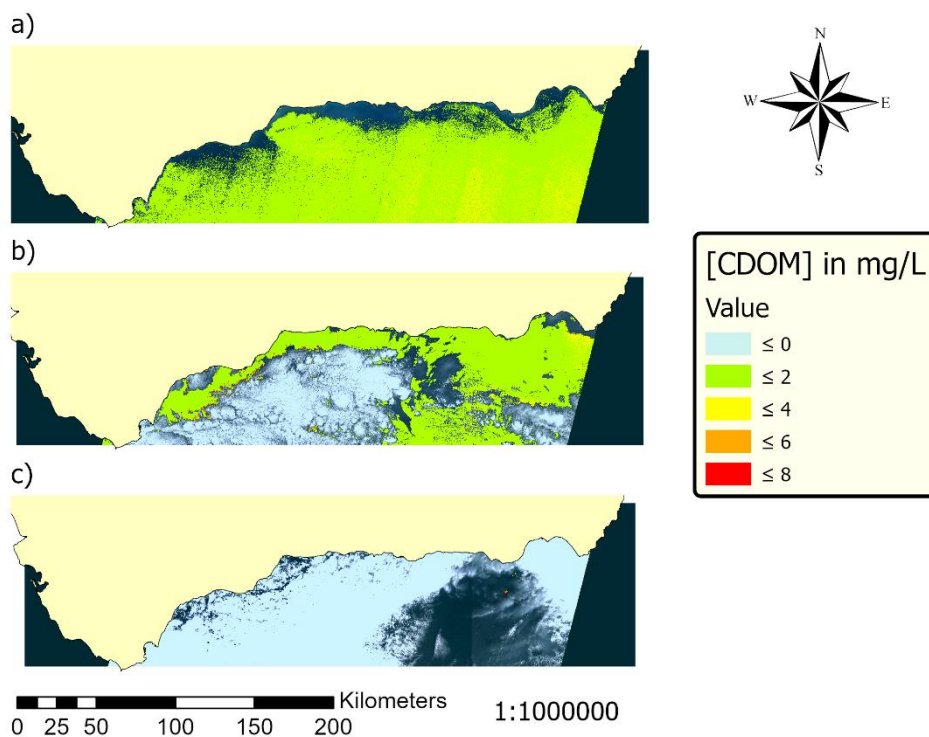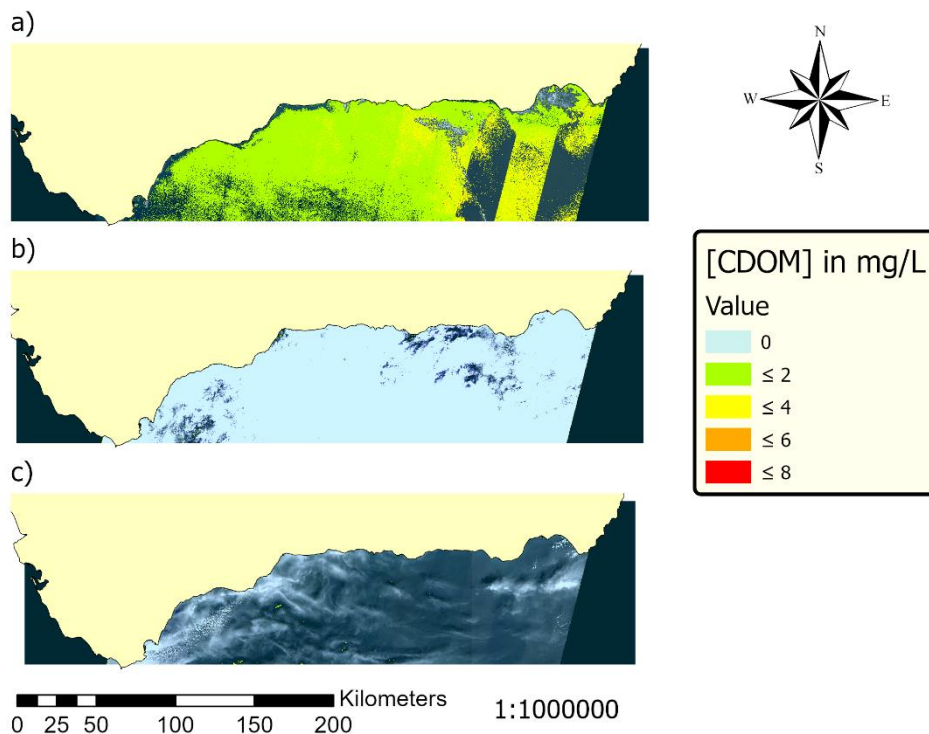

Figure 12: CDOM concentrations for March for which each map represents a) March 4th, b) March 14th and c) March 24th

The CDOM concentrations for April are displayed in Figure 13. When observing this figure, it is to be noticed the large clouds covering the second day (13b), April 14th. Moreover, for the third day (13c), April 24th, some clouds cover the area. Not only they cover the parts which look white, but the sea color can also be seen to be lighter than it is in images without clouds. Therefore, low clouds, which affect the result of the imaging analysis, were present during this day. The only day with complete data is the first day (13a), April 4th.

This day (13a) presents some errors due to the satellite images used being slightly compromised. This can be seen in the right of the image, which shows lines in which the values are much lower than expected compared to those around them. This is not a natural limit; it is an error due to the source data (the satellite images) being compromised. It can be seen in most of the images; nevertheless, in this one, the effect is more notable. Even with the error, concentration values of 0 mg/L to 2 mg/L can be seen in almost all the sea. Furthermore, concentrations on the 2 mg/L to 4 mg/L range can be seen in the eastern part of the sea, similarly to the ones observed in Figures 11c and 12a. The week previous to this date was dominated by heavy storms, as seen in weather tables [66]. This could explain the high concentrations of nearshore.

For April 14th and April 24th there is not much to be analyzed. They both show concentration levels up to 6 mg/L in small areas which could be analyzed between clouds. The weather tables [66] show storms throughout the month, which explains the difficulty in obtaining good satellite imagery.

Overall, this month shows a distribution of the concentrations similar to the one presented in previous dates with high concentrations. It was a rainy month, thus providing little data due to the clouds covering two of the three images available to the public from this satellite.

Figure 13: CDOM concentrations for April for which each map represents a) April 3rd, b) April 13th and c) April 23rd
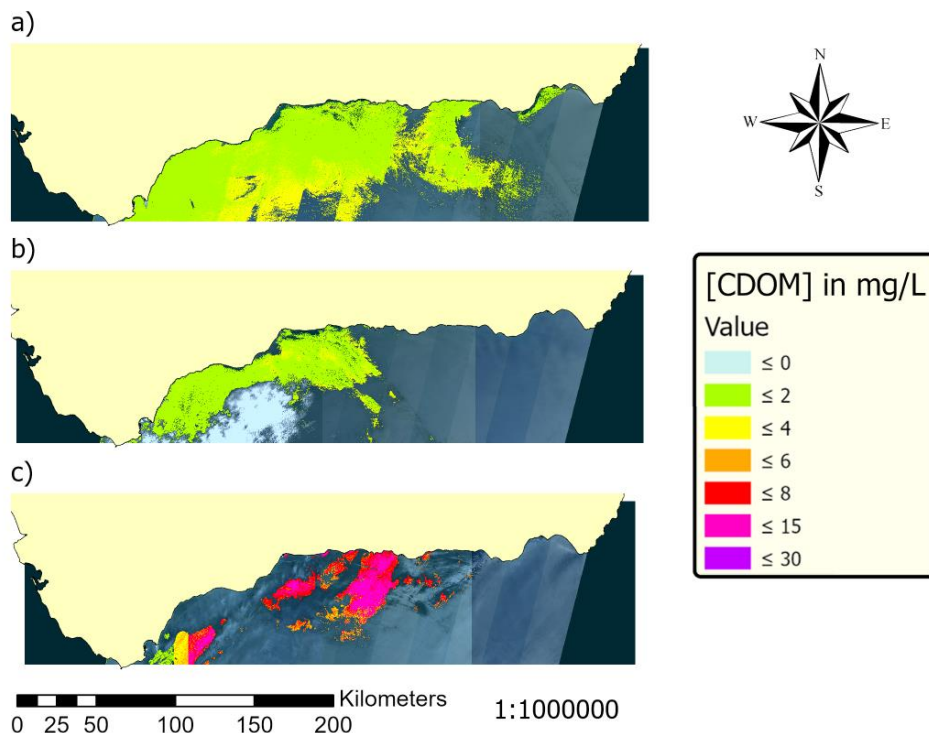
For May, the CDOM concentrations are presented in Figure 14. This is the first month in which all three days can be studied without major clouds interfering. The first day (14a), May 4th, has a clear sky, as does the third day (14c), May 24th. The second day (14b), May 14th, presents some clouds on the western part of the Alboran Sea, close to the Strait of Gibraltar. It is to be noted that on May 24th the concentrations got higher, two new ranges had to be added. Concentrations from 8 mg/L to 15 mg/L are shown in pink while those from 15 mg/L to 30 mg/L are shown in purple.

The concentration levels for May 4th shows a distribution close to the coast and with higher concentrations at the center-western offshore waters. This can be explained due to the storms from the week before [66]. The heavy rain causes massive overland flows, which would explain CDOM levels. This is seen on April 4th as well (Figure 13a).

For May 14th it is important to remark the lower presence of storms the week before [66]. Thus, we can see retreatment in the distribution of CDOM levels. Nevertheless, we can see how the CDOM is moving to the east, with concentrations being higher on the eastern part of the patch of CDOM. For this week, half of the study area was on Phase 1. Next week all of Andalusia was on Phase 1.

The week previous to the third day, May 24th, there were storms again. Moreover, temperatures started being higher [66]. The results presented in Figure 14c show the highest CDOM concentrations of all. This is certainly a CDOM peak, which is to be expected around spring. It can be caused due to the storms combined with the temperature increase. Those parameters can affect the physicochemical properties and its ecosystem, thus making the degradation of CDOM slower.

The results from this month show a seasonal peak. Moreover, it is important to mention that after this month, half of the study area entered Phase 2.

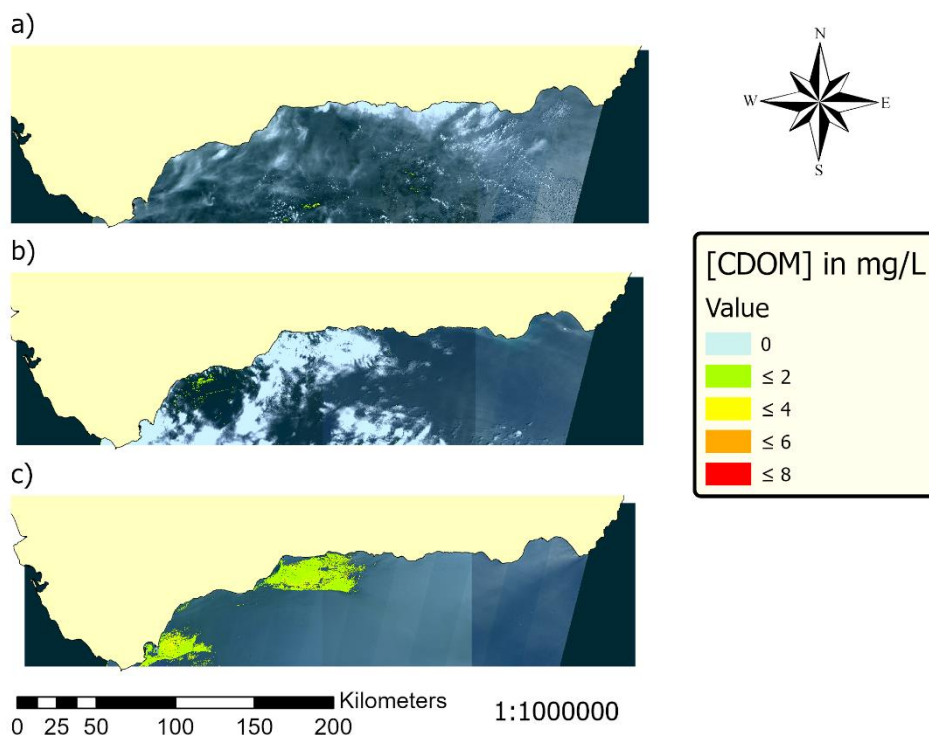**Figure 14:** CDOM concentrations for May for which each map represents a) May 3rd, b) May 13th and c) May 23rd

Finally, the concentrations of CDOM for June are shown in Figure 15. The first day (15a), June 2nd, is hard to study due to the clouds which seem to be similar to those on April 23rd. For the second day (15b), June 12th, the situation is similar, although a small area in the west can be seen. The third day (15c), June 22nd, presents a clear sky. It is important to note that on June 1st the entire area entered Phase 2, on June 8th it entered Phase 3, and on June 21st it entered the New Normality.

For June 2nd only some small gaps between clouds can be analyzed. Nevertheless, most of the values for those areas are on the 0 mg/L to 2 mg/L and 2 mg/L to 4 mg/L concentration ranges. This is a drastic decrease considering the values for May 24th (Figure 14c). Nevertheless, ten mostly dry days went by between both images. This linked with other parameters such as temperature, wind, and the physicochemical characteristics of the sea may have caused the decrease.

Next day, June 12th, shows no CDOM in the eastern part of the Alboran Sea. Moreover, the western side presents very small concentrations in areas where the clouds open and the sea can be studied. After this week, marine transportation was allowed on all the national territory and passengers were allowed to embark ferries.

Finally, on June 22nd two very distinctive plumes can be seen heading east. One of them comes from the Algeciras (left) port area while the other comes from the area around Malaga (center). They are the two most important ports in the area of interest. Moreover, the concentrations for this date present a more equal ratio between the ranges 0 mg/L to 2 mg/L and 2 mg/L to 4 mg/L than any other image. This is most likely due to the human factor, the revitalization of marine transportation [1].

This month is difficult to study due to the cloudy weather. Nevertheless, the sudden human impact on the low concentrations before is certainly presented. This illustrates the effect of a sudden change on an ecosystem.

Figure 15: CDOM concentrations for June for which each map represents a) June 2nd, b) June 12th and c) June 22nd

4.2. Suspended particulate matter (SPM)

This sub-section deals with the results concerning the concentrations of SPM. They can be related to the concentrations of CDOM. Since their causes are similar [17]. Nevertheless, SPM levels can increase due to other causes.

For the month of February, as seen in Figure 16, all the days present clouds. The first day (16a), February 3rd only has two small clouds. Then, the second day (16b), February 13th, is mostly covered by them. Finally, the third day (16c), February 23rd, presents clouds mostly on the western side of the Alboran Sea.

The SPM concentrations levels are low and close to the shore and clouds for February 3rd. This distribution does not correlate to the CDOM distribution, thus indicating the cause for those levels is a different one. In comparison to CDOM levels, these are more localized, especially nearshore. Most of the concentration levels for this day are below 6 g/m^3.

Even though not much can be analyzed for February 13th, it is certain that the concentration levels for the small areas between clouds present higher values than the previous day. This correlates with what happened to CDOM, proving the storm caused a massive overland flow, which could explain both SPM and CDOM levels increasing.

For February 23rd all the visible water presents concentrations higher than 2 g/m^3. Some parts on the southeastern area present concentrations up to 10 g/m^3. Moreover, areas close to the clouds and close to the coast have SPM levels up to 14 g/m^3 and even 18 g/m^3.

Overall, we can see that, even though the initial conditions were different, the evolution is similar to the one for CDOM. It is important to note that this first month was before the quarantine started and during winter.
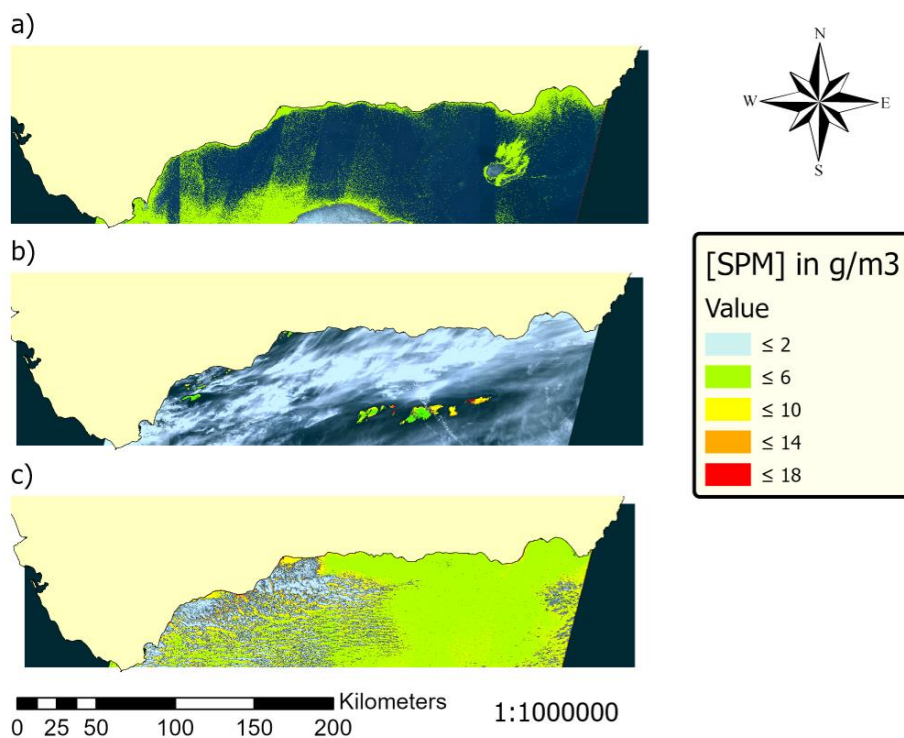
Figure 16: SPM concentrations for February for which each map represents a) February 3rd, b) February 13th and c) February 23rd

The next month to be studied is March, during which the quarantine started. The SPM concentration levels for March can be seen in Figure 17. Out of three days, only the first one (17a), March 4th, presents a clear sky. The next studied day (17b), March 14th, presents clouds, mostly on the western side of the sea. For the third studied day (17c), March 24th, there are more clouds, and only a small part of the sea can be studied.

For March 4th a distribution similar to the one observed on February 23rd (Figure 16c) can be observed. Nevertheless, concentrations seem to peak near Malaga port, with levels up to 18 g/m³. The port activity is a likely cause of this peak. Concentrations are also high nearshore in Cabo de Gata and Almeria (top right corner). Surprisingly enough, concentrations are not that high in Algeciras port.

On March 14th, the day the quarantine started, the concentrations peaked both in the east and west but lowered at the Malaga port. The areas which can be seen between clouds in the west show concentrations in the 2 g/m³ to 6 g/m³ and 6 g/m³ to 10 g/m³ ranges. In the east, values peak around Almeria and Cabo de Gata, reaching concentrations up to 14 g/m³ and even 18 g/m³. Due to the effect of clouds, they seem to not reach the shore near Cabo de Gata, and they do though. This may be caused by dust transported by wind since the week previous to that day had been dry and dust being carried offshore is a natural cause for high SPM concentrations at sea [17].

For March 24th not much can be said. The small gaps between clouds present low concentration levels, unlike CDOM concentrations for this date. Which means that either the overland flows did not contain as much SPM or it did not reach that far.

This month shows high SPM concentration levels for the two days, which could be studied. Said peaks seem to be linked to human activities since they are both nearshore. Moreover, this is the month in which quarantine and spring started.
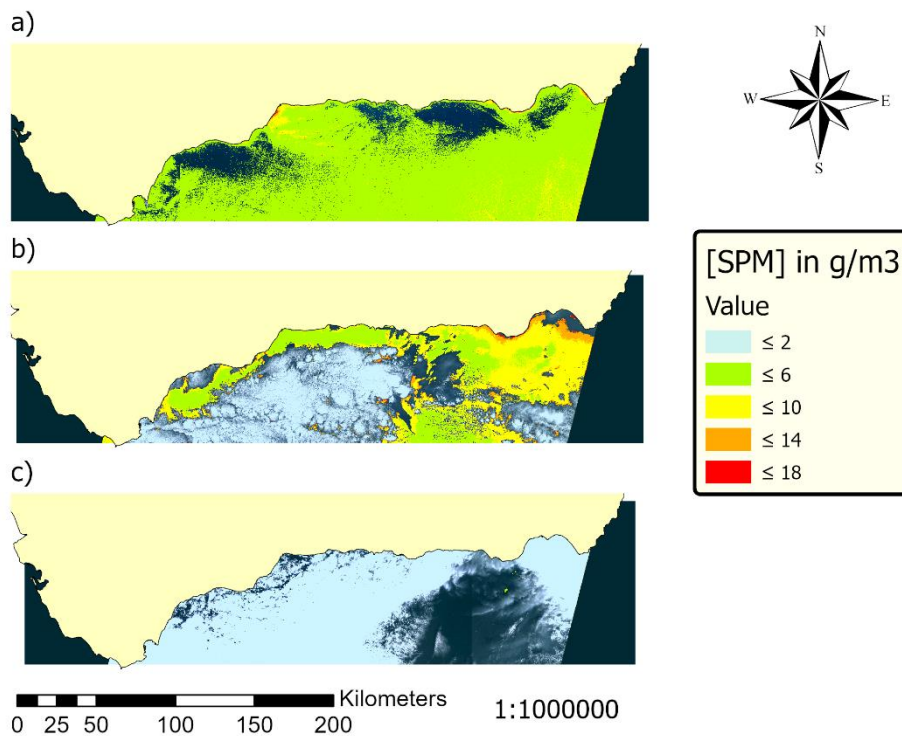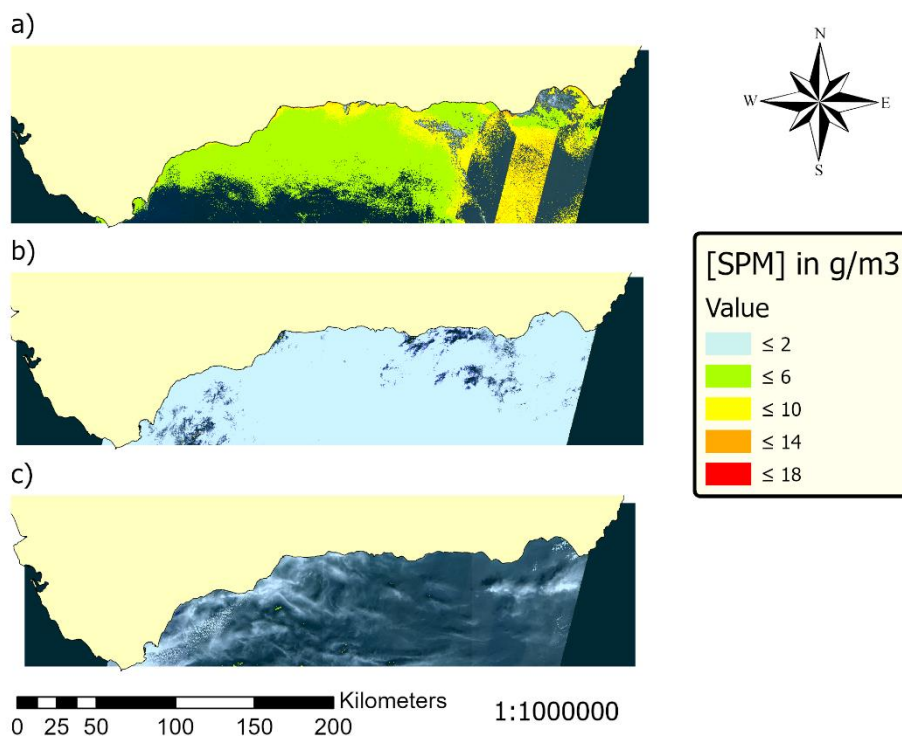

Figure 17: SPM concentrations for March for which each map represents a) March 4th, b) March 14th and c) March 24th

April is probably the hardest month to describe since two of its days present such a cloud density that it is practically impossible to analyze them. Nevertheless, the results from this month are presented in Figure 18. The first day (18a) has a clear sky, although, as explained in 4.1. the eastern sub-area file is compromised. Clouds cover most of the sky for the second day (18b), April 14th, and the third day (18c), April 24th. Thus, the data from those days is almost inexistent.

The concentration levels for April 3rd are higher on the eastern side of the Alboran Sea. It is a shame since it is the area for which the file was corrupted and could not compute the entire image. Nevertheless, the increased concentration can be seen. Most of the concentration values for that area reach 10 g/m^3. Concentrations are higher nearshore, going up to 14 g/m^3. This reinforces the possibility of the peaks being due to dust carried through the wind. Concentrations of CDOM were also higher on the southeastern side for this date, although they were not present nearshore. This seems to be a constant for SPM though, its presence nearshore even though the detection concentration has been increased to 2 g/m^3.

For April 13th some small gaps between clouds can be seen, for which the average concentration seems to be in the 10 g/m^3 to 14 g/m^3. This increase may have to do with the storms which hit the month of April according to the weather tables [66]. The next studied day, April 23rd presents lower concentrations, most of them on the 2 g/m^3 to 6 g/m^3 range. This may have to do with hydrological conditions caused by the storms on the week previous to that date [66].

Overall, this month is hard to analyze and try to figure out the concentration dynamics, since both there are clouds and the image for April 4th is compromised. Nonetheless, all data can be used, and therefore it has been analyzed and explained in this section.

Figure 18: SPM concentrations for April for which each map represents a) April 3rd, b) April 13th and c) April 23rd

The concentration levels for SPM in May are shown in Figure 19. This is the first month for which almost all the areas can be analyzed without cloud interference. The first studied day (19a), May 3rd, has clear skies and the concentration levels can be studied without any interference. The next studied day (19b), May 13th, presents some lose clouds on the western side of the sea. Nevertheless, they cover a little fraction of the area of interest. Finally, the third day (19c), May 23rd, presents some light clouds.

The concentration levels for May 3rd seem to have moved from those on April 3rd. SPM presence is no longer on the eastern part of the Alboran Sea, and now the higher values are on the western side. Although most of the values are on the 2 g/m^3 to 6 g/m^3 range, values from the 6 g/m^3 to 10 g/m^3 and 10 g/m^3 to 14 g/m^3 ranges can be seen offshore. The week previous to this date presents high precipitation levels [66]. CDOM presented high concentration levels on that area as well for this date. This could indicate a massive overland flow which has already gone far into the sea and carries SPM.

For May 13th the concentrations seem to have lowered, although they are close to the western side as well. Their distribution is similar to the CDOM distribution for this date, reinforcing the possibility of the concentration levels being caused by storms. Since the week before May 13th there were fewer storms, this could cause lower concentration levels for this date. It is important to note that on May 11th, half of the study area entered Phase 1.

The concentration levels for May 23rd seem to have lowered to mostly values from 2 g/m^3 to 6 g/m^3. Nonetheless, SPM has spread in distribution, covering areas which were not covered on May 13th. This, once again, may have to do with winds. It is important to note that on May 18th, the entirety of the study area entered Phase 1.

This month, in which Andalusia entered Phase 1, seems to show the consequences of a massive overland flow caused by a storm.
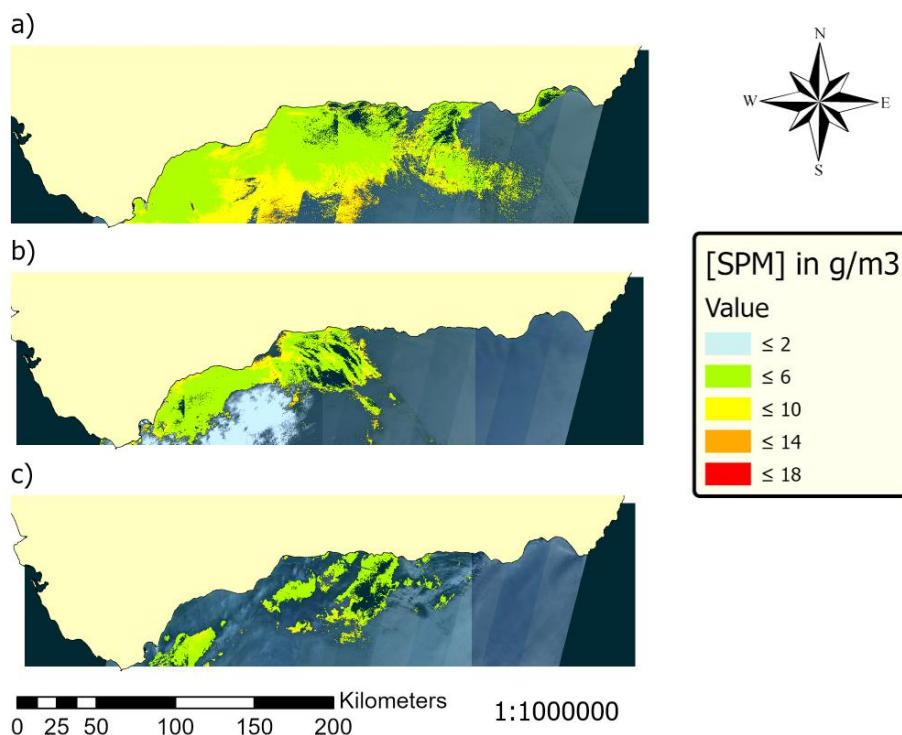
Figure 19: SPM concentrations for May for which each map represents a) May 3rd, b) May 13th and c) May 23rd

June is the last month to be studied and, like April, it presents some difficulties. The first studied day (20a), June 2nd, presents thin clouds which difficult the process of estimating water parameters using satellite imagery. This is also a problem for the second studied day (20b), June 12th. Nevertheless, this date presents a small opening on the western side. Finally, the last day (20c), June 22nd, had clear skies and can be easily studied.

Most of the data for June 2nd cannot be analyzed due to the clouds covering the sea. Nonetheless, for the small gaps in which the imaging techniques could be run, the values presented are mostly on the 2 g/m^3 to 6 g/m^3 range. On this date, all of Andalusia was already on Phase 2.

On June 8th, the area of interest entered Phase 3. Although data from June 12th cannot be analyzed as well as data from other days, it shows low concentration values. Most of them are on the 2 g/m^3 to 6 g/m^3 range and do not cover the full extent of the opening between clouds.

Finally, on June 22nd, a day after the end of quarantine, during the New Normality, the concentration values peaked. It is interesting to note that their distribution is very similar to the distribution of CDOM for this date. They are higher near the Algeciras port and the Malaga port. Especially on the Algeciras area, for which values on the 10 g/m^3 to 14 g/m^3 range can be seen. The other concentration levels present on this date have values on the 2 g/m^3 to 6 g/m^3 and 6 g/m^3 to 10 g/m^3 ranges. It is important to note that on this date, many restrictions regarding marine transportation had been lifted [1]. Taking this into account and observing both peaks near important ports, it is easy to assert the cause. Moreover, both plumes have similar behavior, and they drift to the east.

This final month presents evidence of human activities affecting SPM levels on seawater ecosystems.
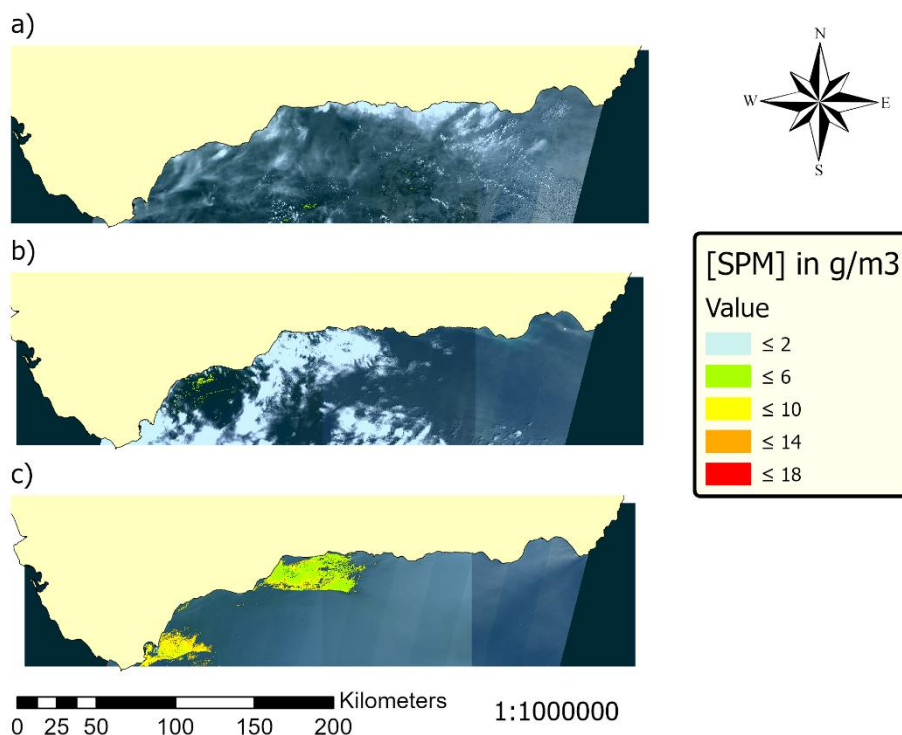
Figure 20: SPM concentrations for June for which each map represents a) June 2nd, b) June 12th and c) June 22nd

4.3. Chlorophyll a (Chl-a)

In this sub-section, the dynamics of Chl-a levels on the Alboran Sea are presented. High Chl-a levels can be naturally caused by storms and high nutrient loads [18], presenting a correlation with high CDOM and SPM levels.

During the first month studied for this project, February, some difficulties were found. All the days present cloudy conditions, nevertheless, this is only an important issue for the second day (21b), February 13th. The clouds present on the first day (21a), February 3rd, are small and localized. Moreover, the clouds on the third day (21c), February 23rd, cover the western side and are lose clouds with spaces between them.

The Chl-a levels for February 3rd present mostly concentrations lower than 50 µg/L. Nonetheless, this date presents higher concentrations near the clouds as well as some higher concentrations near the Malaga port and the Strait of Gibraltar. Concentrations present on these areas go up to 100 µg/L. Chl-a is present everywhere on the area of study.

For February 13th not much can be studied. Nevertheless, the areas visible through the clouds, present concentration levels with most values lower than 25 µg/L. Although concentration levels did not change much, the coverage increased. This could be caused by a storm, as explained for the CDOM and SPM concentrations for this date.

On February 23rd both higher concentrations and a larger presence of Chl-a can be seen. Most concentration levels are lower than 50 µg/L. Nevertheless, there seem to be more peaks of concentration levels on the 50 µg/L to 75 µg/L and 75 µg/L to 100 µg/L ranges than for the first day. This could easily be the aftermath of a series of storms [66].

On this winter month, the Chl-a dynamics seem to be correlated to storms, presenting an increase.
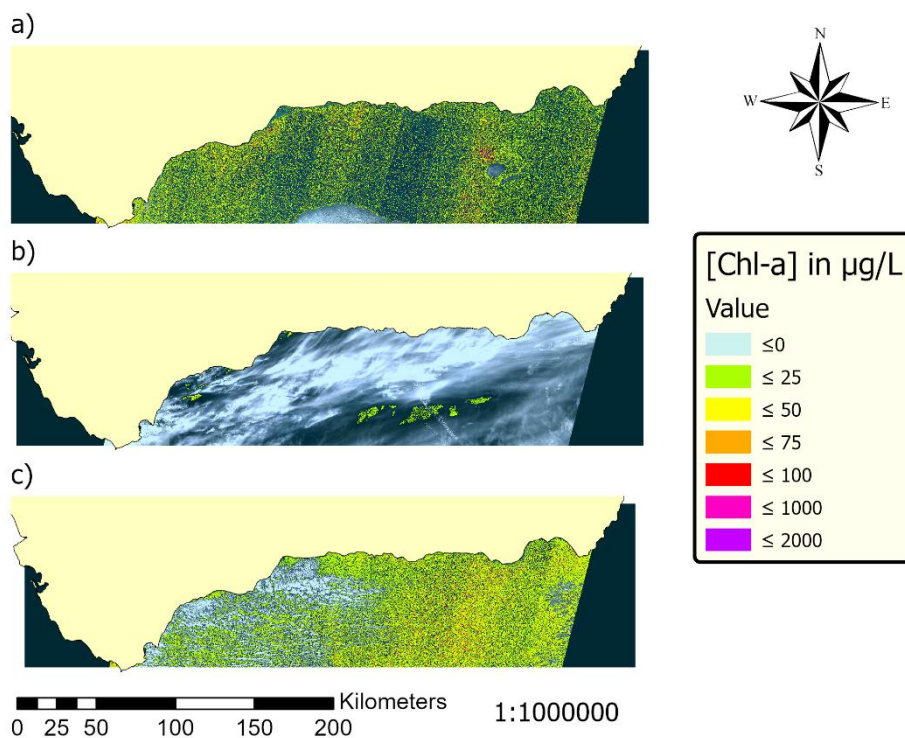
Figure 21: Chl-a concentrations for February for which each map represents a) February 3rd, b) February 13th and c) February 23rd
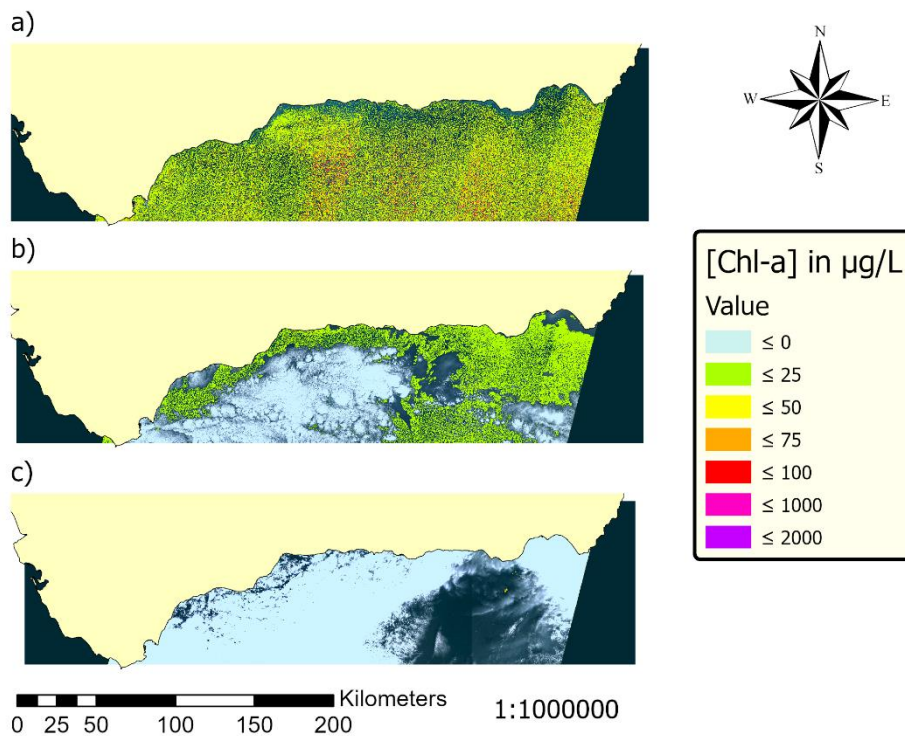
For the month of March, the Chl-a concentration levels are shown in Figure 22. The first day studied for this month (22a), March 4th, presents clear skies and all the area can be studied. This is not the case for the two other days studied for this month. The second one (22b), March 13th, presents clouds on the western and southern sides of the area. Moreover, the third day (22c), March 23rd, presents clouds covering most of the area, mostly thick clouds, but also thinner clouds.

March 4th shows a scenario similar to February 24th (Figure 21c), although the Chl-a levels close to the coast seem to have reduced. Most concentration levels present values lower than 50 µg/L for this date. Nevertheless, there are more areas with concentrations up to 100 µg/L than there was the previous day. CDOM presented higher concentrations for this date as well.

For March 14th, the concentrations seem to have lowered, most of them fall on the 0 µg/L to 25 µg/L range. Nonetheless, their distribution thickens on the eastern side of the sea. This correlates to SPM and CDOM concentration levels increase for this date. It is possible that the dust which could have caused the SPM unusually high levels contained a high proportion of nutrients. It is important to note that this date is the day the quarantine started.

Next, March 24th cannot be interpreted. The only data available is from small gaps between clouds. The concentration levels for these openings present values on the 25 µg/L to 50 µg/L range. This is probably caused by the storms which hit Andalusia during this period. CDOM concentrations peaked for this date as well.

On this month, for which both the quarantine and spring started, the values seem to show the aftermath of a storm. The consequences of later storms cannot be seen due to cloud coverage.

Figure 22: Chl-a concentrations for March for which each map represents a) March 4th, b) March 14th and c) March 24th

Next comes April, its Chl-a concentration levels are shown in Figure 23. It is the hardest to analyze the month due to the weather conditions. It was a rainy month, according to the weather tables [66]. This causes two out of three days to be covered in clouds. Thick clouds for the second day (23b), April 13th, and thin clouds for the third day (23c), April 23rd. Moreover, for the first day (23a), April 3rd, the data on the eastern sub-area is compromised from its source. Nonetheless, as long as there are data, the results are analyzed.

For April 3rd concentration levels mostly on the 0 µg/L to 25 µg/L range can be seen throughout the entire area. Said area presents concentration levels on the 25 µg/L to 50 µg/L as well, less though. In a similar way to SPM and CDOM, the higher concentration levels for this date are on the eastern side of the Alboran Sea. In this case, there are some areas for which the concentration gets to 75 µg/L. The week before this date presented rains, this increase could be caused by those storms.

Next, April 13th presents little to no data. The points for which concentrations were calculated between clouds present concentrations on the 0 µg/L to 25 µg/L range mostly, and some on the 25 µg/L to 50 µg/L range. The spatial distribution of the Chl-a cannot be studied for either this date nor the next.

Then, the concentration levels which can be studied for April 23rd present mostly values on the 0 µg/L to 25 µg/L range. Contrary to April 13th, this date presents concentrations higher than 50 µg/L, on the 50 µg/L to 75 µg/L range. This sudden increase most likely had to do with the storms, and the massive overland flows caused by them.

Overall, in this spring month dominated by storms, the trend observed in March can be observed for April 3rd. The next two days cannot be thoroughly analyzed.
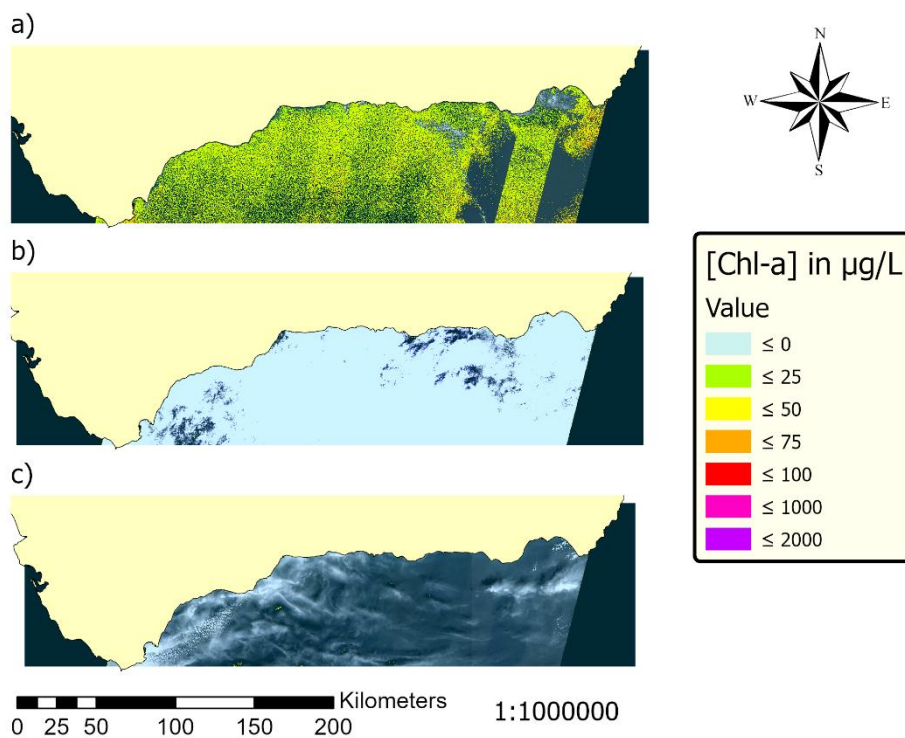
Figure 23: Chl-a concentrations for April for which each map represents a) April 3rd, b) April 13th and c) April 23rd

Following, the next month analyzed is May. The Chl-a concentration values for the said month can be seen in Figure 24. For this month, the first two studied days (24a and 24b), May 3rd and May 13th can be analyzed without major complications. May 13th presents clouds on the western side, they are small and compact though. Nevertheless, the third studied day (24c), May 23rd, presents some thin clouds which difficult the study.

The first studied day, May 3rd, presents concentration levels mostly on the 0 µg/L to 25 µg/L range. Nonetheless, near to the Algeciras port, concentration levels increase to the 25 µg/L to 50 µg/L range. Furthermore, some values near the coastline on the center and eastern parts of the sea present concentration levels up to 75 µg/L. These levels are not only present there, also on the plume on the east. On May 11th, half of the area of interest entered Phase 1.

For May 13th the concentration levels have mostly reduced both in magnitude and dispersion. During this period, there were fewer storms, which could explain these values. The concentration levels for Chl-a present for this day correlate to the levels for CDOM and SPM as well. Increases in concentration levels for all these parameters can be naturally caused by storms. Therefore, this retreating behaviour can be interpreted as the consequence of a storm period. On May 18th, all of Andalusia entered Phase 1.

The week previous to May 23rd was dominated by heavy rains [66]. This could explain the higher concentration values presented in the central area for this date. These concentrations increased up to 100 µg/L and, on some parts, even 1000 µg/L and 2000 µg/L. This is an unprecedented peak for the time-period studied for this project. Moreover, it correlates with the CDOM peak. This reinforces the possibility of the peak being caused by a massive overland flow due to the storms.

This month presents a peek at its end, after an intense storm period. Moreover, it was in this month when Andalusia entered Phase 1.
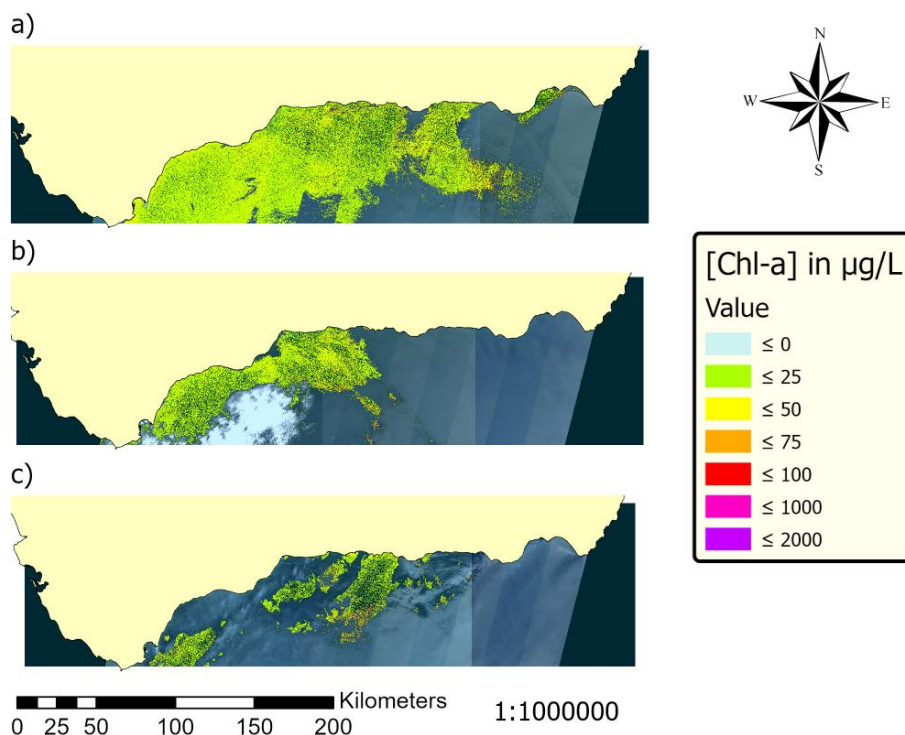
Figure 24: Chl-a concentrations for May for which each map represents a) May 3rd, b) May 13th and c) May 23rd

Finally, the last month is June. The Chl-a concentration levels for this month can be seen in Figure 25. This month is hard to study, similarly to April, since two of its days are almost fully covered by clouds. For the first studied day (25a), June 2nd, there are thin clouds. The next studied day (25b), June 12th, clouds are a bit denser and offer some openings. The only day which can be fully studied is the last one (25c), June 22nd. During this month Andalusia entered Phase 2, Phase 3 and the New Normality.

The values for June 2nd were taken a day after Phase 2 started in Andalusia. It presents concentrations up to 100 µg/L for the small gaps between clouds, which could be caused by precipitations.

On June 8th all of Andalusia entered Phase 3. Therefore, the values for June 12th correspond to this period. Recreational fishing was permitted, and recreational sailing was allowed within the territorial unit [1]. Concentration levels and distribution on the gap on the western side of the Alboran Sea are low and spare. The Chl-a levels show almost no Chl-a in comparison to the levels before the quarantine (Figure 21a).

Finally, for June 22nd, barely a day after the instauration of the New Normality, two plumes can be seen. One of them seems to come from the Algeciras port while the other comes from the Malaga Port. Taking into account the revitalization of marine traffic the day before it is easy to interpret these plumes as a result of said traffic. Chl-a concentration levels for the Algeciras port plume are on the 0 µg/L to 25 µg/L, and 25 µg/L to 50 µg/L ranges mostly. In contrast, Chl-a concentration levels for the Malaga port plume reach up to 1000 µg/L and presents many values on the 75 µg/L to 100 µg/L range. These peaks, which are present in CDOM and SPM concentration levels for this date as well, are undoubtedly caused by human activities.

This month shows the effects of a sudden anthropogenic change in an ecosystem which had been undisturbed for months.
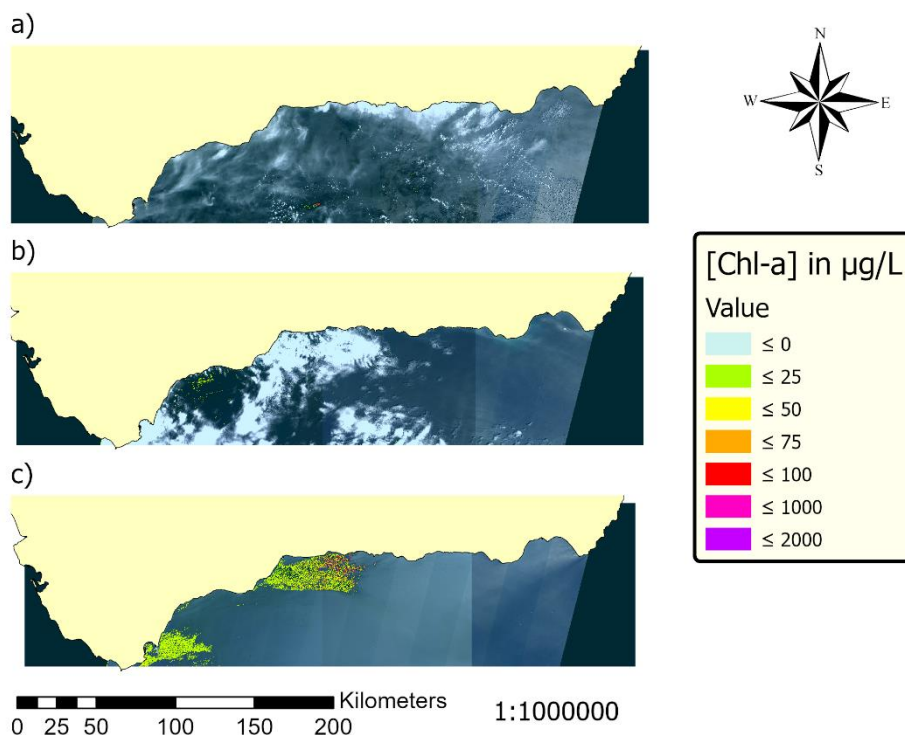
Figure 25: Chl-a concentrations for June for which each map represents a) June 2nd, b) June 12th and c) June 22nd

4.4. Harmful algal blooms (HABs)

The analysis of the distribution for HABs throughout the studied time-period is different from the analysis for CDOM, SPM and Chl-a. There were only three HAB episodes on the five months studied for this project. Nevertheless, Figures 26 to 30 show the results for each of the days analyzed. It is important to note the brevity of HABs [19]. The HABs represented on this project may not be all the blooms which happened during this period of time.

The first and most notorious bloom is in February 3rd (Figure 26a). The HAB distribution corresponds with the Chl-a distribution for that date. The values here show a clear HAB, big enough to cover the entire Alboran Sea. The first week of February presents temperatures higher than usual [66] which, added to the usually high nutrient content on this season [67], could have caused the bloom. This correlates with climate change as well. This happened before the quarantine.

The second bloom happened on April 4th (Figure 28a), close to the Strait of Gibraltar. It does not match with high Chl-a levels nor with high CDOM or SPM levels. This could indicate the algal class [68]. The bloom, nevertheless, seems to come from the strait, probably being caused by a nutrient load entering the Mediterranean Sea.

The last noticeable bloom is on May 3rd (Figure 29a). It matches up with high Chl-a concentrations as well as the presence of CDOM and SPM. Therefore, it is similar to the bloom on February 3rd. It is most likely due to the high nutrient load present on the sea after the storms which hit Andalusia the week before [66]. Both this HAB and the on April 4th happened during Phase 0.

It is important to note that, although for June 22nd all concentrations are high near the Algeciras port and the Malaga port, a HAB cannot be seen. Nevertheless, after just one day of marine trafficking, it is to be expected. The nutrients are already there and looking closer, and some red spots can be seen near the Malaga port.
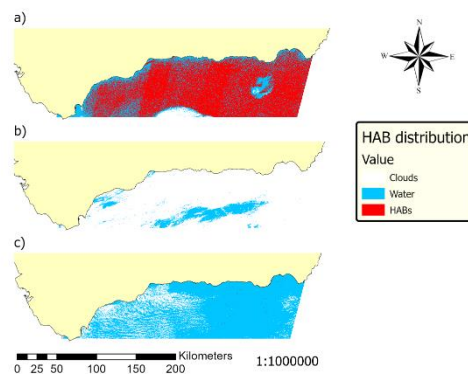
Figure 26: HABs for February for which each map represents a) February 3rd, b) February 13th and c) February 23rd
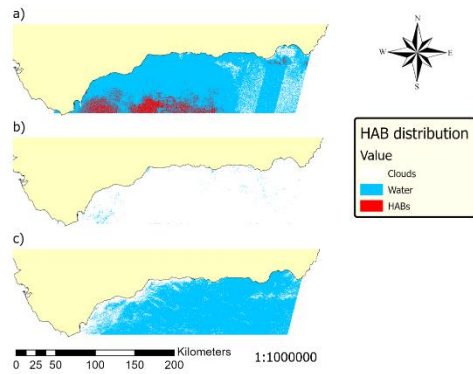
Figure 27: HABs for April for which each map represents a) April 3rd, b) April 13th and c) April 23rd
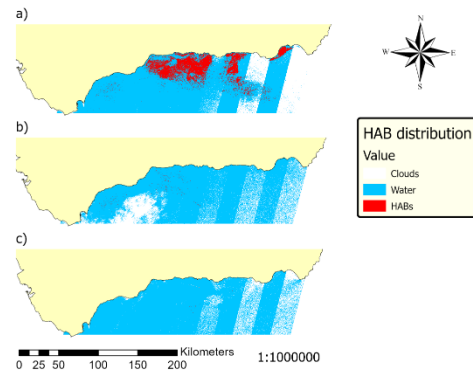
Figure 28: HABs for May for which each map represents a) May 3rd, b) May 13th and c) May 23rd

4.5. Summary of the observed dynamics

The dynamics observed are presented in Figure 29. Increases are shown in color red, whereas decreases are shown in color green. Those days for which the concentration levels were similar to the days before are shown in yellow. Moreover, the HABs are represented in red, and the rains are represented in different shades of blue depending on their intensity. The first day for CDOM, SPM and Chl-a is marked in red to indicate their presence.

It is to be noted that most increase days during the quarantine happened after an intense storm period. Moreover, the quarantine period presents more days with a decreasing trend, especially for May and June, after the rainy season. This season being the last week of March, and the month of April. Two out of three HABs correlate with high CDOM, SPM and Chl-a concentration levels, the outlier may be caused by a nutrient load entering from the Atlantic Ocean. Furthermore, on June 22nd, barely a day after the New Normality was established, an increase can be observed.

	February			March			April			May			June		
	3	13	23	4	14	24	3	13	23	3	13	23	2	12	22
CDOM															
SPM															
Chl-a															
HAB															
Rain															

Figure 29: Summary of the dynamics
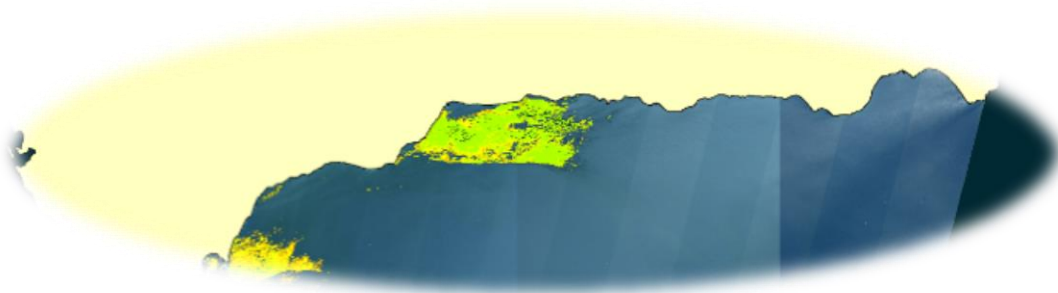
5. Conclusions

5.1. Fulfilment of the objective

The MOs of this project were the study and accurate portrayal of the environmental status of the Alboran Sea right before and during the COVID-19 quarantine. This has been achieved through the analysis of satellite imagery using several software in order to produce indices for a series of environmental parameters. The parameters have been compared with one another and with weather tables [66] to determine the causes of concentration peaks.

For several of the days studied the CDOM, SPM and Chl-a concentrations peaked and showed a similar distribution. This is most likely due to the storms on the week previous to each date, causing a massive overland flow. This happened undoubtedly for February 23rd, March 14th, April 3rd and May 3rd. In fact, for May 3rd a HAB was observed as well. HABs are short-spanned phenomena which explain why only three HABs have been observed in this experience.

Moreover, the aftereffects and how the concentrations lower and disperse after a storm can be observed in several of the days. After the storm on February 13th the concentration of CDOM, SPM and Chl-a peaked in February 23rd. The evolution of these parameters can be seen on March 4th. Furthermore, after the rains on May 3rd, the concentration levels lower on May 13th.

February 3rd is a unique day. It presents the biggest HAB, as well as high Chl-a and CDOM concentrations showing a distribution similar to the HAB. It also presents SPM distributed nearshore. The HAB was most likely caused by the high temperatures [66] and the nutrient-rich waters [67] and influenced the Chl-a and CDOM readings. Two more HAB have been observed, one of them, on May 3rd, related to the storms. The other HAB, on April 3rd, does not correlate to the CDOM, SPM nor Chl-a concentration levels nor distribution. This HAB is close to the Strait of Gibraltar and could have been caused by nutrient-rich waters entering the Mediterranean Sea.

The highest peak for CDOM was on May 23rd, reaching values up to 30 mg/L. For SPM, the peak happened on March 14th although other days reached up to 18 g/m^3 as well. The highest Chl-a values can be observed on May 23rd. There were only 3 observed HABs during the period. Nevertheless, the most extended one was on February 3rd.

June 22nd is an interesting date. It is barely a day after quarantine finished, the port activity was being reactivated. CDOM, SPM and Chl-a concentrations peaked for this day near the Malaga port and the Algeciras port. This proves the impact of human activity in an environment which had been undisturbed for several months. SPM had already peaked near the Malaga port on March 4th, before the quarantine started, further proving the human impact of ports.

5.2. Repercussion

This study is unprecedented since never in recent history had Spain been subjected to quarantine. The lack of human activities in the sea provided us with data for the study of unperturbed marine environmental dynamics in an already human-modified environment. This can be key in restoration and recovery studies. Moreover, this study further proves the usefulness of satellite imagery for the monitoring of marine environments.

Furthermore, the impact after just one day of human activities on an environment which had been unperturbed for months has been observed. This plays a crucial role in understanding the magnitude this kind of impacts has. Not only for monitoring, for raising people's awareness as well.

5.3. Difficulties found during the process

The COVID-19 changed the world in which we live and work. Reunions had to be online, and doubts had to be expressed through email instead of just going to the directors' offices. And whenever the student had to go to the lab to work on another computer, security measures had to be followed.

The effects of COVID-19 are not only physical. The stress generated by the sanitary situation was added to the usual stress this kind of projects (end-of-master/end-of-degree projects) puts students through. It was hard having to focus on working when the future, in terms of everyday life, is uncertain.

The technical difficulties the student found while working on this project are fully explained on Annex III.

5.4. Personal opinion

When the COVID-19 quarantine started, I was devastated to know I could not work on the project I had already planned with my directors. Said project required a lot of laboratory work, and I was not going to be able to do it. Nevertheless, one of my directors, Lorena, suggested the idea of working with remote sensing to check the effects quarantine had on the marine environment. I liked the idea. I am fond of working with satellite imagery. Nevertheless, that was not the only reason. Choosing to work with what we have, to turn a distressing situation into an opportunity to learn and to raise environmental awareness. I found strength in that. And I found that, among the chaos and the horrible things which were happening, which are still happening, choosing to try to make something good out of it gave me hope. And I think this project has helped me deal with the situation we are going through.

5.5. Future research and applications

This project further proved the usefulness of satellite imagery for environmental monitoring. The possible future projects split in two directions.

The first direction would be the continuation of monitoring marine environments. Combining the use of Sentinel-2 and Landsat-8 in like other researchers have done before [49-50]. This would yield data from more days, reducing the time between two datasets. Furthermore, other indices could be tested, even some original indices comparing their results to the observed in-situ values (from buoys). Moreover, this could be done for other places rather than just the Alboran Sea. For exemple, for the Balear Sea or the entire Spanish eastern coast.

Next, the use of satellite imagery for environmental monitoring during the COVID-19 quarantine could be applied to other ecosystems. Forests, lakes, wetlands and even the air quality can be monitored through remote sensing. It would be interesting to check the effect a prolonged underexposure to human activities could have on these environments. Moreover, it could help us understand the dynamics and processes which happen on these places.

It is important to note that, although some conference papers were to be created with the data from this project, this was not possible due to the quarantine. Nevertheless, it is going to be turned into a journal paper. It is not clear yet to which journal it is going to be summited.

REFERENCES

1. Paul, V., Shekharaiah, P. C., Kushwaha, S., Sapre, A., Dasgupta, S., & Sanyal, D. (2020). Role of Algae in CO 2 Sequestration Addressing Climate Change: A Review. In *Renewable Energy and Climate Change* (pp. 257-265).

2. O'Hara, C. C., Villaseñor-Derbez, J. C., Ralph, G. M., & Halpern, B. S. (2019). Mapping status and conservation of global at-risk marine biodiversity. *Conservation Letters*, 12(4), e12651.

3. Alonso, R. R., & Aja, A. H. (2015). *La construcción del espacio litoral*. El caso de la costa de Cartagena (Doctoral dissertation, Universidad Politécnica de Madrid).

4. Gössling, S., Hall, C. M., & Scott, D. (2018). Coastal and ocean tourism. In *Handbook on marine environment protection* (pp. 773-790).

5. van Beusekom, J. E. (2018). Eutrophication. In *Handbook on Marine Environment Protection* (pp. 429-445).

6. Gallo, F., Fossi, C., Weber, R., Santillo, D., Sousa, J., Ingram, I., & Romano, D. (2018). Marine litter plastics and microplastics and their toxic chemicals components: the need for urgent preventive measures. *Environmental Sciences Europe*, 30(1), 13.

7. Khalil, M. A., & Ahmied, E. K. (2019). Steel Corrosion Control in Seawater Using Zinc sacrificial anode. *Journal of Pure and Applied Sciences*, 18(2).

8. España. Orden TMA/419/2020, de 18 de mayo, por la que se actualizan las medidas en materia de ordenación general de la navegación marítima adoptadas durante el estado de alarma para la gestión de la crisis sanitaria ocasionada por el COVID-19 al proceso de desescalada. BOE, 19 de mayo de 2020, núm. 141, p. 33496-33503

9. RTVE. *El mapa de la desescalada en España: así ha sido el camino a la nueva normalidad en cada provincia.* <https://www.rtve.es/noticias/20200622/mapa-desescalada-espana-fase-esta-tu-provincia/2013477.shtml> [Consulta: 07 de agosto de 2020]

10. Kumari, C. U., Samiappan, D., Kumar, R., & Sudhakar, T. (2019). Fiber optic sensors in ocean observation: A comprehensive review. *Optik*, 179, 351-360

11. Jury, M. R., & Goschen, W. S. (2020). Physical ocean-atmosphere variability over the shelf of South Africa from reanalysis products. *Continental Shelf Research*, 104135.

12. Pai, I. K., & Govekar, K. (2016). An extensive study on physico-chemical parameters of Bay of Bengal and Central Indian Ocean Basin.

13. Wollschläger, J., Voß, D., Zielinski, O., & Petersen, W. (2016). In situ observations of biological and environmental parameters by means of optics—development of next-generation ocean sensors with special focus on an integrating cavity approach. IEEE Journal of Oceanic Engineering, 41(4), 753-762.

14. Ludvigsen, M., & Sørensen, A. J. (2016). Towards integrated autonomous underwater operations for ocean mapping and monitoring. *Annual Reviews in Control*, 42, 145-157.

15. Slonecker, E. T., Jones, D. K., & Pellerin, B. A. (2016). The new Landsat 8 potential for remote sensing of colored dissolved organic matter (CDOM). *Marine pollution bulletin, 107*(2), 518-527.

16. Novoa, S., Doxaran, D., Ody, A., Vanhellemont, Q., Lafon, V., Lubac, B., & Gernez, P. (2017). Atmospheric corrections and multi-conditional algorithm for multi-sensor remote sensing of suspended particulate matter in low-to-high turbidity levels coastal waters. *Remote Sensing, 9*(1), 61.

17. Kang, L., He, Y., Dai, L., He, Q., Ai, H., Yang, G., ... & Li, H. (2019). Interactions between suspended particulate matter and algal cells contributed to the

reconstruction of phytoplankton communities in turbulent waters. *Water research, 149*, 251-262.

18. Pérez-Ruzafa, A., Campillo, S., Fernández-Palacios, J. M., García-Lacunza, A., García-Oliva, M., Ibañez, H., ... & Sala-Mirete, A. (2019). Long-Term dynamic in nutrients, chlorophyll a, and water quality parameters in a coastal lagoon during a process of eutrophication for decades, a sudden break and a relatively rapid recovery. *Frontiers in Marine Science, 6*, 26.

19. Gobler, C. J. (2020). Climate change and harmful algal blooms: insights and perspective. *Harmful Algae, 91*, 101731.

20. Giardino, C., Brando, V. E., Gege, P., Pinnel, N., Hochberg, E., Knaeps, E., ... & Foerster, S. (2019). Imaging spectrometry of inland and coastal waters: state of the art, achievements and perspectives. *Surveys in Geophysics*, 40(3), 401-429.

21. ESA SENTINEL ONLINE. *Sentinel Overview* <https://sentinel.esa.int/web/sentinel/missions> [Consulta: 18 de agosto de 2020]

22. COPERNICUS EUROPE'S EYES ON EARTH. *Copernicus in Brief* <https://www.copernicus.eu/en/about-copernicus/copernicus-brief> [Consulta: 18 de agosto de 2020]

23. ESA SENTINEL ONLINE. *Collaborative Ground Segment* <https://sentinel.esa.int/web/sentinel/missions/collaborative;jsessionid=22DBBDCA C07302DB41C83C1720BFBD35.jvm1> [Consulta: 18 de agosto de 2020]

24. ESA SENTINEL ONLINE. *Thematic Areas* <https://sentinel.esa.int/web/sentinel/thematic-areas;jsessionid=22DBBDCAC07302DB41C83C1720BFBD35.jvm1> [Consulta: 18 de agosto de 2020]

25. ESA SENTINEL ONLINE. *Sentinel-2* <https://sentinel.esa.int/web/sentinel/missions/sentinel-2;jsessionid=22DBBDCAC07302DB41C83C1720BFBD35.jvm1> [Consulta: 18 de agosto de 2020]

26. Sozzi, M., Marinello, F., Pezzuolo, A., & Sartori, L. (2018, July). Benchmark of satellites image services for precision agricultural use. In *Proceedings of the AgEng Conference, Wageningen, The Netherlands* (pp. 8-11).

27. Soñes Bori, J. (2020). Coastal bathymetry from satellite high resolution monitoring.

28. Ruiz Fernández, L. Á., Estornell Cremades, J., & Erena Arrabal, M. (2017, October). Teledetección. Nuevas plataformas y sensores aplicados a la gestión del agua, la agricultura y el medio ambiente. In *Colección Congreso*. Editorial Universitat Politècnica de València.

29. Pinto Santos, P. (2016). *Estudio geomorfológico en los entornos costeros con mareas mediante la extracción automática de líneas de costa de imágenes de satélite de resolución media* (Doctoral dissertation).

30. Tamburini, C., Canals, M., de Madron, X. D., Houpert, L., Lefèvre, D., Martini, S., ... & Al Samarai, I. (2013). Deep-sea bioluminescence blooms after dense water formation at the ocean surface. *PloS one*, *8*(7), e67523.

31. Toming, K., Kutser, T., Laas, A., Sepp, M., Paavel, B., & Nõges, T. (2016). First experiences in mapping lake water quality parameters with Sentinel-2 MSI imagery. Remote Sensing, *8*(8), 640.

32. Orlandi, M., Silvio Marzano, F., & Cimini, D. (2018). Remote sensing of water quality indexes from Sentinel-2 imagery: development and validation around Italian river estuaries. *EGUGA*, 19808.

33. Caballero, I., Steinmetz, F., & Navarro, G. (2018). Evaluation of the first year of operational Sentinel-2A data for retrieval of suspended solids in medium-to-high-turbidity waters. *Remote Sensing*, 10(7), 982.

34. Balasubramanian, S. V., Pahlevan, N., Smith, B., Binding, C., Schalles, J., Loisel, H., ... & Bunkei, M. (2020). Robust algorithm for estimating total suspended solids (TSS) in inland and nearshore coastal waters. *Remote Sensing of Environment*, 111768.

35. Li, P., Ke, Y., Bai, J., Zhang, S., Chen, M., & Zhou, D. (2019). Spatiotemporal dynamics of suspended particulate matter in the Yellow River Estuary, China during the past two decades based on time-series Landsat and Sentinel-2 data. *Marine pollution bulletin*, 149, 110518.

36. Liu, H., Li, Q., Shi, T., Hu, S., Wu, G., & Zhou, Q. (2017). Application of sentinel 2 MSI images to retrieve suspended particulate matter concentrations in Poyang Lake. *Remote Sensing*, 9(7), 761.

37. Saberioon, M., Brom, J., Nedbal, V., Souček, P., & Císař, P. (2020). Chlorophyll-a and total suspended solids retrieval and mapping using Sentinel-2A and machine learning for inland waters. *Ecological Indicators*, *113*, 106236.

38. Hafeez, S., & Wong, M. S. (2019, July). Measurement of Coastal Water Quality Indicators Using Sentinel-2; An Evaluation Over Hong Kong and the Pearl River Estuary. In IGARSS 2019-2019 *IEEE International Geoscience and Remote Sensing Symposium* (pp. 8249-8252). IEEE.

39. Potes, M., Rodrigues, G., Penha, A. M., Novais, M. H., Costa, M. J., Salgado, R., & Morais, M. M. (2018). Use of Sentinel 2–MSI for water quality monitoring at Alqueva reservoir, Portugal. *Proceedings of the International Association of Hydrological Sciences*, *380*, 73-79.

40. Ha, N. T. T., Thao, N. T. P., Koike, K., & Nhuan, M. T. (2017). Selecting the best band ratio to estimate chlorophyll-a concentration in a tropical freshwater lake using sentinel 2A images from a case study of Lake Ba Be (Northern Vietnam). *ISPRS International Journal of Geo-Information, 6*(9), 290.

41. Khalili, M. H., & Hasanlou, M. (2019). Harmful Algal Blooms Monitoring Using SENTINEL-2 Satellite Images. *The International Archives of Photogrammetry, Remote Sensing and Spatial Information Sciences, 42*, 609-613.

42. Alba, G., Anabella, F., Marcelo, S., Andrea, G. A., Ivana, T., Guillermo, I., ... & Michal, S. (2019, July). Spectral Monitoring of Algal Blooms in an Eutrophic Lake Using Sentinel-2. In *IGARSS 2019-2019 IEEE International Geoscience and Remote Sensing Symposium* (pp. 306-309). IEEE.

43. Pahlevan, N., Sarkar, S., Franz, B. A., Balasubramanian, S. V., & He, J. (2017). Sentinel-2 MultiSpectral Instrument (MSI) data processing for aquatic science applications: Demonstrations and validations. *Remote sensing of environment, 201*, 47-56.

44. Bande, P., Adam, E., Elbasit, M. A. A., & Adelabu, S. (2018, July). Comparing landsat 8 and sentinel-2 in mapping water quality at vaal dam. In *Proceedings of the International Geoscience and Remote Sensing Symposium (IGARSS), Valencia, Spain* (pp. 22-27).

45. Pahlevan, N., Chittimalli, S. K., Balasubramanian, S. V., & Vellucci, V. (2019). Sentinel-2/Landsat-8 product consistency and implications for monitoring aquatic systems. *Remote sensing of Environment, 220*, 19-29.

46. Peterson, K. T., Sagan, V., & Sloan, J. J. (2020). Deep learning-based water quality estimation and anomaly detection using Landsat-8/Sentinel-2 virtual constellation and cloud computing. *GIScience & Remote Sensing, 57*(4), 510-525.

47. Caballero, I., & Navarro, G. (2018, July). Retrieval of Suspended Solids from Landsat-8 and Sentinel-2: A Tool for Coastal Monitoring in Extremely Turbid Waters. In *IGARSS 2018-2018 IEEE International Geoscience and Remote Sensing Symposium* (pp. 7874-7877). IEEE.

48. Xu, J., Fang, C., Gao, D., Zhang, H., Gao, C., Xu, Z., & Wang, Y. (2018). Optical models for remote sensing of chromophoric dissolved organic matter (CDOM) absorption in Poyang Lake. *ISPRS Journal of Photogrammetry and Remote Sensing,*

142, 124-136.

49. Cao, F., Tzortziou, M., Clark, B., & Hood, R. R. (2019). Dissolved organic carbon dynamics at tidal wetlands-estuary interface: Observations from Landsat-8/OLI and Sentinel-2 MSI. *AGUFM, 2019*, H31N-1952.

50. Chen, J., Zhu, W., Tian, Y. Q., & Yu, Q. (2020). Monitoring dissolved organic carbon by combining Landsat-8 and Sentinel-2 satellites: Case study in Saginaw River estuary, Lake Huron. *Science of The Total Environment, 718*, 137374.

51. Kostianoy, A. G., Soloviev, D. M., Kostianaia, E. A., Đurović, B., & Pestorić, B. (2016). Satellite remote sensing of the Boka Kotorska Bay. In *The Boka Kotorska Bay Environment* (pp. 495-520). Springer, Cham.

52. Ogashawara, I. (2019). The use of Sentinel-3 Imagery to monitor cyanobacterial blooms. *Environments, 6*(6), 60.

53. Khan, F. A., Khan, T. M. A., & Uddin, M. G. (2019). Satellite based Monitoring of Interactions between Chl-a and SST in the Arabian Sea and Persian Gulf area: a useful tool to identify ocean productive zones. *Journal of Space Technology, 9*(1).

54. Benallal, M. A., Moussa, H., Lencina-Avila, J. M., Touratier, F., Goyet, C., El Jai, M. C., ... & Poisson, A. (2017). Satellite-derived CO2 flux in the surface seawater of the Austral Ocean south of Australia. *International Journal of Remote Sensing, 38*(6), 1600-1625.

55. Schaeffer, B. A., Iiames, J., Dwyer, J., Urquhart, E., Salls, W., Rover, J., & Seegers, B. (2018). An initial validation of Landsat 5 and 7 derived surface water temperature for US lakes, reservoirs, and estuaries. *International Journal of Remote Sensing, 39*(22), 7789-7805.

56. COPERNICUS OPEN ACCESS HUB. *Home* <https://scihub.copernicus.eu/dhus/#/home> [Consulta: 01 de agosto de 2020]

57. ESA SENTINEL ONLINE. *Level-1* <https://sentinel.esa.int/web/sentinel/user-guides/sentinel-2-msi/processing-levels/level-1> [Consulta: 21 de agosto de 2020]

58. MUSEUM. *ACOLITE* <https://odnature.naturalsciences.be/remsem/software-and-data/acolite> [Consulta: 18 de agosto de 2020]

59. Vanhellemont, Q. (2019). Adaptation of the dark spectrum fitting atmospheric correction for aquatic applications of the Landsat and Sentinel-2 archives. *Remote Sensing of Environment*, 225, 175-192.

60. Vanhellemont, Q., & Ruddick, K. (2016, May). Acolite for Sentinel-2: Aquatic applications of MSI imagery. In *Proceedings of the 2016 ESA Living Planet Symposium, Prague, Czech Republic* (pp. 9-13).

61. ESRI. *ArcGIS Pro* <https://pro.arcgis.com/es/pro-app/get-started/install-and-sign-in-to-arcgis-pro.htm> [Consulta: 01 de agosto de 2020]

62. ARCGIS DESKTOP. *Mosaic To New Raster* <https://desktop.arcgis.com/en/arcmap/latest/tools/data-management-toolbox/mosaic-to-new-raster.htm> [Consulta: 01 de agosto de 2020]

63. ARCGIS DESKTOP. *Raster Calculator* <https://desktop.arcgis.com/es/arcmap/latest/tools/spatial-analyst-toolbox/raster-calculator.htm> [Consulta: 01 de agosto de 2020]

64. Nechad, B., Dogliotti, A., Ruddick, K., & Doxaran, D. (2016, August). Particulate backscattering retrieval from remotely-sensed turbidity in various coastal and riverine turbid waters. In *Proc. Living Planet Symposium* (ed. Ouwehand, L.), ESA-SP (Vol. 740).

65. Moses, W. J., Gitelson, A. A., Berdnikov, S., Saprygin, V., & Povazhnyi, V. (2012). Operational MERIS-based NIR-red algorithms for estimating chlorophyll-a concentrations in coastal waters—The Azov Sea case study. *Remote Sensing of Environment,* 121, 118-124.

66. JUNTA DE ANDALUSIA CONSEJERÍA DE AGRICULTURA, GANADERIA, PESCA Y DESARROLLO SOSTENIBLE. *Temperaturas y precipitaciones semanales*

AEMET <
https://www.juntadeandalucia.es/organismos/agriculturaganaderiapescaydesarrollo
sostenible/servicios/estadistica-cartografia/estadisticas-
agricolas/paginas/estadisticas-aemet.html> [Consulta: 27 de agosto de 2020]

67. Del Carmen García-Martínez, M., Vargas-Yáñez, M., Moya, F., Santiago, R., Muñoz, M., Reul, A., ... & Balbín, R. (2019). Average nutrient and chlorophyll distributions in the western mediterranean: Radmed project. *Oceanologia, 61*(1), 143-169.

68. Binding, C. E., Zastepa, A., & Zeng, C. (2019). The impact of phytoplankton community composition on optical properties and satellite observations of the 2017 western Lake Erie algal bloom. *Journal of Great Lakes Research, 45*(3), 573-586.